Simplifying the interaction of land surfaces with radiation for relating remote sensing products to climate models

B. Pinty and T. Lavergne

Global Vegetation Monitoring Unit, IES, EC Joint Research Centre, Ispra (VA), Italy

R. E. Dickinson

School of Earth and Atmospheric Sciences, Georgia Institute of Technology, Atlanta, Georgia, USA

J.-L. Widlowski, N. Gobron, and M. M. Verstraete

Global Vegetation Monitoring Unit, IES, EC Joint Research Centre, Ispra (VA), Italy

[1]   Remote sensing products, such as the fraction of reflected solar radiation flux, as well as the amount of radiation absorbed in the photosynthetically active spectral region and the Leaf Area Index (LAI), are operationally available from Space Agencies. Climate models may benefit from these products provided their one dimensional (1-D) radiation transfer schemes effectively represent the three dimensional (3-D) effects implied by the internal spatial variability of vegetation canopies, e.g., the leaf area density, at all scales and resolutions involved (say from 1 to 100 kilometers). Failing to do so leads to inherent inconsistencies between the domain-averaged reflected and absorbed fluxes, and the implied Leaf Area Index. We propose a comprehensive approach which introduces a parameterization of the internal variability of the LAI in the 1-D representation of the radiation scheme, called a domain-averaged structure factor, and provides a description of the radiant fluxes fully consistent with the LAI specified by remote sensing. We take this opportunity to revisit and update the two-stream formulations implemented in climate models to accurately estimate the fractions of radiation absorbed separately by the vegetation canopy and the underlying surface. This is achieved by isolating the contributions of the vegetation canopy alone, the background as seen through the canopy gaps and the multiple scattering between the vegetation layer and the background. The performance of this formulation is evaluated against results from Monte Carlo simulations relative to explicit realistic 3-D canopies to show that the proposed scheme correctly simulates both the amplitude and the angular variations of all radiant fluxes with respect to the solar zenith angle.

Citation: Pinty, B., T. Lavergne, R. E. Dickinson, J.-L. Widlowski, N. Gobron, and M. M. Verstraete (2006), Simplifying the interaction of land surfaces with radiation for relating remote sensing products to climate models, *J. Geophys. Res.*, *111*, D02116, doi:10.1029/2005JD005952.

1. Introduction

[2] General Circulation Models (GCMs) are designed to simulate the likely evolution of the weather and climate on the basis of physical processes as well as initial and boundary conditions. To do so, these models must represent the exchanges of energy (radiation and heat) momentum and mass (water, carbon and other chemical species) between the atmosphere and the underlying surface, in particular terrestrial environments. The longer the simulation period, the greater the detail and accuracy needed in representing these processes. Yet, for practical reasons,

e.g., resolution issues, numerical stability considerations and computational limitations, small scale processes are generally parameterized in terms of larger scale variables [e.g., *Dickinson et al.*, 1986; *Verstraete and Dickinson*, 1986; *Avissar and Verstraete*, 1990; *Sellers et al.*, 1997]. Direct observations of the geophysical system thus play critical roles either in defining its initial state, or in specifying changes in forcings, or as a tool to evaluate the pertinence and accuracy of the predictions.

[3] Over the past decade, Space Agencies such as the European Space Agency's ENVISAT programme (http://www.esa.int) and the U.S. National Aeronautics and Space Administration's EOS programme (http://eospso.gsfc.nasa.gov/) have demonstrated the feasibility of systematically and repetitively acquiring measurements of the radiative

environment of the planet in a range of spectral and directional conditions. To the extent GCMs can explicitly represent these radiation quantities, such observational data can be used in a process known as assimilation, where the state variables describing the system in the model are adjusted so that the model estimates the measurements as closely as possible. Alternatively, algorithms are developed and implemented in the operational ground segments of these Agencies to derive higher level products describing the properties of components of the geophysical system, such as the albedo of land surfaces [e.g., *Schaaf et al.*, 2002; *Diner et al.*, 2005], the Fraction of Absorbed Photosynthetically Active Radiation (FAPAR) [e.g., *Gobron et al.*, 1999], the Leaf Area Index (LAI) [e.g., *Myneni et al.*, 2002], amongst others. GCMs should thus periodically ingest these operational products to update the corresponding boundary conditions.

[4] How climate models interface with the information derived from space measurements thus becomes a rather critical issue. In the simpler cases, climate models use predefined land cover maps as an indexing tool to specify a variety of land surface properties, such as albedo, roughness, and many others. More sophisticated models include an explicit module describing the entire set of physical processes and exchanges at scales and resolutions appropriate for the host model [e.g., *Dickinson et al.*, 1986; *Sellers et al.*, 1996; *Burke et al.*, 2000] although many of the basic variables describing the surface may still be defined a priori, on the basis of look-up tables. This latter category of models thus ensures that (1) the fluxes are simulated using state variables available from recent remote sensing products such as the LAI, (2) the various radiant fluxes estimated by the model are consistent with products such as LAI, FAPAR and surface albedo, derived from remote sensing and, ultimately, (3) the fluxes of radiation, heat, water, momentum are properly balanced. The radiation transfer schemes that are used to simulate these processes in climate models and to retrieve high level products from remote sensing data should be compatible with each other or radiatively equivalent with respect to the radiant fluxes they generate [e.g., *Verstraete and Pinty*, 1997], although they rarely are. Incompatibilities between the assumptions and approximations implicitly made by using different models, e.g., one-dimensional (1-D) versus three-dimensional (3-D) radiation transfer models, may generate discrepancies and biases when remote sensing products are heedlessly ingested by the climate models, as will be seen below.

[5] The most advanced representation of terrestrial surface processes in climate models is confined to simplistic modules implementing one dimensional (vertical) exchange models, in particular with respect to the transfer of radiation. The radiation component of these 1-D modules relies on solutions derived from two-stream approaches [e.g., *Dickinson*, 1983; *Sellers*, 1985; *Dozier*, 1989]. The latter often capitalize on developments made in the field of atmospheric physics [e.g., *Coakley and Chylek*, 1975; *Meador and Weaver*, 1980]. The transfer of radiation in plant canopies is rendered complicated because the elementary scatterers, i.e., the leaves are large compared to the typical wavelength of solar radiation, they can be oriented and clumped and they exhibit complex variable optical properties. The two-stream formulations thus have to be adapted to

represent, at least in simplified forms, the effects of these complexities. In some instances, the proposed solutions require the strict equality between the reflectance and the transmittance of leaves, and are accurate only for leaves with all orientations of equal probability [e.g., *Sellers*, 1985]. In other instances, the multiple scattering processes, particularly significant in the near-infrared spectral region, are parameterized (as opposed to represented explicitly as a function of the relevant state variables) [e.g., *Zeng et al.*, 2002; *Zhou et al.*, 2003; *Dai et al.*, 2003] and not fully accounted for in the case of spatially heterogeneous environments [e.g., *Niu and Yang*, 2004; *Yang et al.*, 2001].

[6] The control of the radiation transfer regime by vegetation architecture and its spatial heterogeneity may be partly acknowledged by some of the retrieval algorithms used to derive remote sensing products. For example, the LAI/FAPAR estimations derived from MODIS and MISR measurements are based on 3-D radiation transfer models [*Knyazikhin et al.*, 1998b]. The nature of the physical problem to be solved in that instance fully justifies using such 3-D instead of simpler 1-D models [e.g., *Gerard and North*, 1997; *Knyazikhin et al.*, 1998a; *Panferov et al.*, 2001; *Widlowski et al.*, 2001a; *Rautiainen et al.*, 2004]. An immediate implication of this fact is that the retrieved state variable values, e.g., LAI, cannot be used as such in the 1-D radiation scheme of a GCM since this yields significantly erroneous assessment of the absorbed, transmitted and reflected fluxes. This issue has recently been explored by *Pinty et al.* [2004], who proposed a relatively straightforward approach to the estimation of these radiant fluxes at the satellite pixel resolution through the use of effective (instead of true) variable values. This study also showed that the same principle applies to all state variables of the radiation transfer problem if one is to ensure the correct balance between the three radiant fluxes. For example, the values of effective LAI appropriate for 1-D models should be smaller than the true values by a factor varying from 0.3 for sparse to 0.8 for dense forest canopies, while the leaf single scattering albedo must be simultaneously decreased, and the backscattering efficiency significantly enhanced in the near-infrared spectral domain. This LAI reduction factor in *Pinty et al.* [2004] is a smooth function of the Sun zenith angle and, for randomly dispersed aggregation of leaves, i.e., tree crowns, its effect is somewhat analogous to a clumping factor [e.g., *Nilson*, 1971; *Chen et al.*, 1997a, 1997b]. The need to account for such 3-D induced effects thus introduces an additional information parameterizing the internal variability of the LAI into the 1-D representation of the radiation transfer problem namely, a domain-averaged structure factor.

[7] Since 1-D models will continue to be used to represent surface processes in climate models for the foreseeable future, the practical outcomes of these findings are that (1) the formulation of the two-stream schemes of radiation transfer must be revisited and adapted to use effective variables so as to correctly represent the effect of structure and heterogeneity within the grid cell, (2) the net effect of using these effective variables must be quantitatively assessed, and (3) mechanisms must be proposed to derive the correct values of these effective variables on the basis of their true values, as measured locally or retrieved from a detailed analysis of remote sensing data. These three points

will be explicitly addressed in this paper, though the latter will only be investigated using 3-D simulations.

2. A Two-Stream Based Scheme for 1-D and 3-D Vegetation Canopies

[8] Radiation transfer schemes suitable for GCMs must meet numerous constraints including computer efficiency and robustness, they must use measurable or retrievable variables or parameters and provide sufficiently accurate estimations of the radiant fluxes. For all practical purposes, it is enough to establish appropriate sets of equations permitting us to estimate jointly two only out of the three fluxes which are either reflected, transmitted or absorbed. Indeed at low spatial resolutions, which are more likely to satisfy the conditions imposed by a "radiatively independent volume" [*Pinty et al.*, 2004], these three fluxes are linked by the conservation law, i.e., they sum up to 1 over a black background, independent of the canopy structure prevailing inside and outside the domain.

[9] Radiation schemes should therefore be able to simulate accurately both the flux reflected from the top of the canopy, that is its albedo, and the flux transmitted to the background underneath the vegetation layer in order to estimate the fractions of radiation absorbed separately by the vegetation canopy and the underlying surface. It is noteworthy that these flux estimates have to fully account for the lower boundary contribution, i.e., the background, so that challenging conditions corresponding for instance to snow surfaces can be addressed as well. In this modeling context, the albedo and the fraction of absorbed radiation are key quantities since they affect the climate system and both can be derived reliably at the appropriate spatial and temporal resolutions from measurements gathered by the recent satellites operating in the solar domain. These two quantities are thus prime candidates for upcoming or ongoing validation and assimilation exercises.

2.1. Parameterization of the Surface Albedo With Respect to the Direct and Diffuse Illumination Sources

[10] The albedo (transmission factor) of a geophysical system such as a vegetation canopy layer is defined as a ratio of the upwelling (downwelling at the bottom of the canopy noted z_{bgd}) to the downwelling radiant fluxes at the top of the canopy noted z_{toc}, both depending on the location of the source, i.e., the cosine of the Sun zenith angle, μ_0) and type of illumination (normally both direct and diffuse). The retrieval of this flux ratio from space borne sensors is, however, hindered by the coupling between the intrinsic surface and atmospheric scattered fluxes [*Martonchik et al.*, 1998; *Schaaf et al.*, 2002; *Pinty et al.*, 2005]. Solving this coupled problem imposes the adoption of assumptions or simplifications in the representation of the surface albedo. The most popular one is that the surface albedo is approximated by a simple weighting of two distinct surface albedo types, each associated with an extreme incident radiation field: the Directional Hemispherical Reflectance (DHR), associated with an incident intensity field which is purely collimated and the Bi-Hemispherical Reflectance (BHR$_{iso}$), associated with an incident intensity field that is purely isotropic. Both of these extreme albedo types are indeed

independent from atmospheric ambient conditions. They can be combined to approximate the surface albedo as follows [*Kondratyev*, 1972; *Lewis and Barnsley*, 1994; *Pinty et al.*, 2005]:

$$\text{BHR}^{\star}(z_{toc}, \mu_0) \simeq \text{DHR}(z_{toc}, \mu_0) f^{\downarrow dir}(z_{toc}, \mu_0) + \text{BHR}_{iso}(z_{toc}) f^{\downarrow diff}(z_{toc}, \mu_0) \quad (1)$$

where the weights, $f^{\downarrow dir}$ and $f^{\downarrow diff}$, sum up to 1, and correspond to the fractions of direct and diffuse to total downward flux density, respectively. This parameterized form for the surface albedo, BHR corresponds to the so-called "Blue sky" albedo. It was shown to be accurate enough for a number of applications [*Lewis and Barnsley*, 1994; *Pinty et al.*, 2005] and can be easily estimated from the operational surface and atmospheric products available, for instance, from the MODIS sensors on board Terra and Aqua platforms.

[11] It can readily be seen from (1) that, for given ambient atmospheric conditions, the surface albedo only requires formulae to estimate the surface DHR and its associated BHR$_{iso}$ from the state variable controlling the radiation transfer regime inside the vegetation canopy layer. Since the BHR$_{iso}$ can easily be deduced from the DHR, the next section of this paper will focus on the latter. The following developments capitalize and expand on the results obtained in a previous study [*Pinty et al.*, 2004].

2.2. Identification of the Main Contributions to the Surface Albedo

[12] It is convenient to decompose the intensity field emerging from the top of a canopy layer into a sum of terms isolating the contributions from the various orders of scattering in the vegetation layer and from the background. Such a decomposition yields the following exact formulation for surface albedo, denoted $R_{coupled}^{total}(z_{toc}, \mu_0)$ and representing the DHR [*Nicodemus et al.*, 1977; *Martonchik et al.*, 2000]:

$$R_{coupled}^{total}(z_{toc}, \mu_0) = R_{veg}^{Coll}(z_{toc}, \mu_0) + R_{bgd}^{UnColl}(z_{toc}, \mu_0) + R_{bgd}^{Coll}(z_{toc}, \mu_0) \quad (2)$$

where the first term, R_{veg}^{Coll}, represents the contribution due to the radiation travelling downward along the solar direction μ_0 that has interacted with the vegetation canopy elements only. This is the so-called Black Background contribution since $R_{coupled}^{total}(z_{toc}, \mu_0) = R_{veg}^{Coll}(z_{toc}, \mu_0)$ in the case of a perfectly absorbing background. This term is primarily controlled by the absorbing and scattering properties of the leaves as well as their density and orientation. The second term, R_{bgd}^{UnColl}, denotes the contribution due to the radiant flux scattered by the background and travelling both downward and upward through the canopy gaps. This contribution whose photons have not collided with any vegetation elements is identified as the Black Canopy contribution since $R_{coupled}^{total}(z_{toc}, \mu_0) = R_{bgd}^{UnColl}(z_{toc}, \mu_0)$ in the case of a perfectly absorbing canopy layer. This contribution is therefore strongly controlled by the vegetation architecture. Unlike the first term, it does not contribute any absorption in the vegetation layer. All other contributions to the total surface albedo are included within the term noted $R_{bgd}^{Coll}(z_{toc}, \mu_0)$ which accounts for the multiple interactions

between the vegetation canopy and the underlying background. Since this term involves more than one scattering event, it is equal to zero in the limit of single scattering by the coupled vegetation-background system and its contribution increases rapidly with the surface background brightness.

[13] Similar decompositions can be conducted for the fraction of the fluxes that are absorbed and transmitted by the vegetation layer with respect to both the direct and diffuse solar illumination although with no contribution from the uncollided radiation for the latter flux. The main advantage of this decomposition lies in the isolation of the contributions involving the background properties. The fluxes associated with the vegetation layer and reaching the background can then be easily identified for further applications, e.g., for computation of the heating rates separately in both media.

2.3. Introduction of Effective Variable Values

[14] The use of effective radiative state variables to express the properties of 3-D vegetation canopy systems guarantees the correct simulation of the scattered, transmitted and absorbed radiant fluxes (in vegetation [*Pinty et al.*, 2004]). This requirement is not specific to vegetation canopy systems but applies, in principle, to all radiative systems with significant 3-D structural effects (in clouds [e.g., *Boissé*, 1990; *Cahalan et al.*, 1994; *Szczap et al.*, 2000; *Cairns et al.*, 2000]). In our approach, the values of the effective variables are estimated by inverting a 1-D radiant flux model against fluxes generated by a 3-D model. This constitutes a very robust approach since (1) it guarantees accurate simulations of the three radiant fluxes when using, in direct mode, these effective values, and (2) it does not require an explicit description and understanding of the complex phenomena arising from the presence of the woody elements that are embedded into the leaf layer and located below the bottom of the leaf layer.

2.3.1. Effective LAI Value

[15] In the limit of the 1-D turbid medium representation of a 3-D heterogeneous vegetation canopy, the Black Canopy contribution in (2) must satisfy the exponential Beer-Bouger-Lambert's law. The exponent entering the extinction law can be expressed as a product of three quantites namely, the domain-averaged LAI of the layer, $\langle LAI \rangle$, the leaf extinction coefficient (which depends on the preferred orientations of the leaves inside the crowns and can be expressed via the so-called Ross's G function [e.g., *Ross*, 1981]) and a structure factor (sometimes called clumping factor at the tree resolution) that is associated with the heterogeneous nature of the canopy volume, $\zeta(\mu_0)$. In this context, *Pinty et al.* [2004] suggested to adopt an effective LAI value, $\widetilde{LAI}(\mu_0)$, given by:

$$\widetilde{LAI}(\mu_0) = \langle LAI \rangle \, \zeta(\mu_0) \qquad (3)$$

[16] When assuming a spherical leaf angle distribution function which implies a leaf extinction coefficient equal to 0.5, the area-averaged optical thickness of the canopy in its 1-D turbid medium representation is simply $\widetilde{LAI}(\mu_0)/2$ [*Pinty et al.* 2004, equation (25)]. The effective LAI, a domain-averaged quantity, is thus forced to satisfy the main constraints associated with a 1-D representation and notably that the leaves are randomly distributed and their orientation is given by a spherical distribution inside the structurally
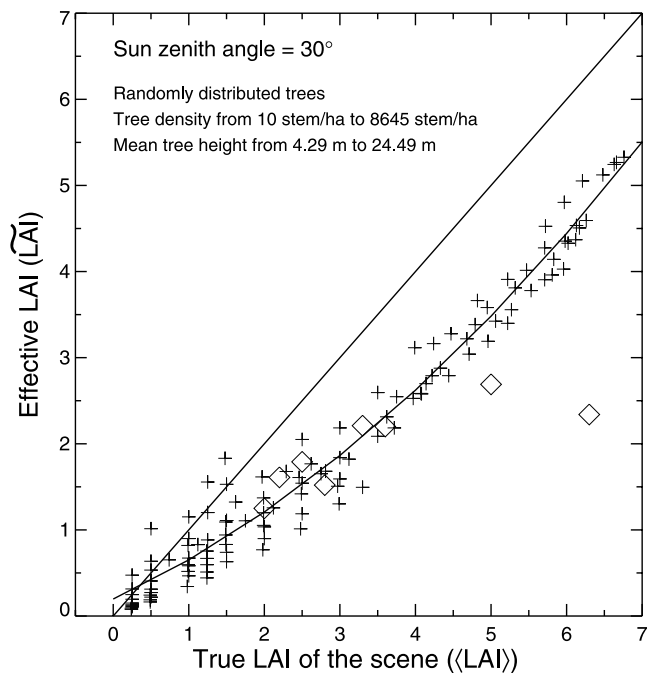
Figure 1. Simulated (pluses) relationship between true and effective LAI values over a wide range of coniferous forest type taken from *Widlowski et al.* [2004]. Field measured (diamonds) values, are taken from the BOREAS experiment after *Chen et al.* [1997b]. The mean relationship between the true and effective LAI values, fitted over the full range of conifer forests, can be approximated by: $\overline{LAI}(\mu_0 = 0.866) \approx 0.197 + 0.40 \times \langle LAI \rangle + 0.05 \times \langle LAI \rangle^2$ (solid line).

homogeneous leaf layer. The introduction of $\zeta \, (\mu_0)$ in (3) can also be seen as the acknowledgement of Jensen's inequality which applies to convex functions [*Jensen*, 1906], that is $\langle \exp \, (-LAI/2\mu_0) \rangle \geq \exp \, (-\langle LAI \rangle / 2\mu_0)$. It is noteworthy that the actual leaf density distribution function may imply some correlation between the positions of the trees, leading non-exponential law decays [e.g., *Nilson*, 1971; *Oker-Blom et al.*, 1991; *Knyazikhin et al.*, 1998a; *Kostinski*, 2001; *Shaw et al.*, 2002; *Davis and Marshak*, 2004] that can still be expressed via the exponential law.

[17] Figure 1 shows the relationships between true and effective LAI to be expected over a wide range of modelled coniferous forest conditions [*Widlowski et al.*, 2004]. The various scenarios considered here are all based on realistic coniferous forest properties as reported in the literature [*Widlowski et al.*, 2003]. The effective LAI values were estimated using the procedure described in *Pinty et al.* [2004] and the radiation directly transmitted to the ground was calculated using the Raytran ray tracing Monte-Carlo model [*Govaerts and Verstraete*, 1998]. Note that the conditions for which the effective LAI values exceed the true values are all associated with canopy conditions exhibiting a very significant amount of woody elements. In these cases, the woody elements contribute significantly to the interception of radiation adding to the value of the effective LAI. This quantity which accounts for all phyto and woody elements composing the vegetation canopy is sometimes called a plant area index. The observed relationships be-

Table 1. Variables Defining the Structurally Heterogeneous Scenes

Variable Identification	Values (Units)
Mean Leaf Area Index over the domain	1.24[S], 2.0[M] and 4.82[D] (m²/m²)
Mean Leaf Area Index of a single tree crown	6.02[S], 6.49[M] and 2.77[D] (m²/m²)
Gap fraction of the scene	0.83[S], 0.69[M] and 0.25[D]
Tree density	53[S], 142[M] and 4718[D] (trees/hectare)
Mean tree height	23.99[S], 24.49[M] and 9.92[D] (m)
Mean tree crown length	7.59[S], 7.09[M] and 7.57[D] (m)
Spatial distribution of tree locations	Poisson distribution
Mean nearest tree distance	8.54[S], 6.25[M] and 1.16[D] (m)
Mean effective domain height[a]	3.93[S], 6.74[M] and 13.86[D] (m)
First order structure function exponent[b]	0.80[S], 0.76[M] and 0.65[D]
Scatterer shape	disc of negligible thickness
Scatterer radius	0.05 (m)
Scatterer normal distribution in tree crown	spherical

[S]Sparse vegetation condition.
[M]Medium vegetation condition.
[D]Dense vegetation condition.
[a]The mean effective domain height is the the mean height of all trees within the domain weighted by their fractional surface coverage [*Widlowski et al.*, 2004].
[b]Derived from statistics of the height fields [*Widlowski et al.*, 2001b].

tween the true and effective LAI values appears to be in good agreement with those deduced from field measurements; the latter result from a careful analysis of multiple estimations collected over multiple locations and tree species during the international Boreal Ecosystem-Atmosphere Study (BOREAS) that have been assembled by *Chen et al.* [1997b, Table 3]. The authors of this data set have already identified the most deviating point ($\langle LAI \rangle > 6$) reported in Figure 1 as an outlier due to large spatial variability and sampling issues over that particular site [*Chen et al.*, 1997b, section 4.2].

[18] As expected, the effective LAI value is generally lower than the domain-averaged true LAI values of the scenes (provided the proportion of woody material is not too large with respect to the green LAI of the scene). Given the limited scatter in the relationship between the effective and true LAI, a second order polynomial can be fitted in order to approximate the anticipated effect due to structure, i.e., $\widetilde{LAI}(\mu_0 = 0.866) = 0.197 + 0.40 \times \langle LAI \rangle + 0.05 \times \langle LAI \rangle^2$, for the general case of coniferous forests.

[19] The dependency of the structure factor $\zeta(\mu_0)$ on the Sun zenith angle was found almost negligible over the range of solar angles that occurred during BOREAS [*Chen et al.*, 1997a, 1997b]. This fact is confirmed by further simulations made, as a function of the Sun zenith angle, for three of the many geophysical scenes used to construct Figure 1. Tables 1 and 2 summarize the geophysical scenarios that were selected to span a range of vegetation densities and spatial distributions. All simulations performed in this context implement an isotropic scattering law for the background and a bi-Lambertian law for the leaf reflectance and transmittance. These three scenes used here (as well as later on to conduct an evaluation of the two-stream solutions) mimic realistic canopy forest scenarios under sparse, medium and dense vegetation conditions over a typical soil background and bright snow in a near-infrared narrow band [e.g., *Painter and Dozier*, 2004]. This high value is chosen on purpose to maximize multiple scattering effects; a value of 0.6 may be more appropriate for broadband calculations in climate models.

[20] Figure 2 illustrates the variations of the structure factor $\zeta(\mu_0)$ as a function of the cosine of the Sun zenith angle $(1 - \mu_0)$. This figure basically suggests that, indeed, the dependency of the structure factor with respect to the Sun zenith angle remains rather smooth and limited (especially for dense canopies illuminated from a solar zenith angle larger than 30°) and can be reasonably well approximated by a linear relationship:

$$\zeta(\mu_0) \approx a + b(1 - \mu_0) \tag{4}$$

where $a = \zeta_{(\mu_0 = 1)}$ is the structure factor corresponding to an overhead Sun. Given that $\exp(-\widetilde{LAI}/2\mu_0) = \exp(-\langle LAI \rangle \zeta(\mu_0)/2\mu_0)$ represents the direct radiation reaching the background level in the 1-D turbid approximation for a Black Canopy, this quantity also expresses the fraction of the background that is directly illuminated for a given vegetation cover noted F_c. This vegetation cover is equal to the ground fractional cover by all vegetation elements accounting for the entire hierarchy of canopy gaps inside the radiatively independent volume. As a consequence, in the particular case of an overhead Sun, $a = \zeta_{(\mu_0 = 1)}$ is also equal to:

$$\zeta_{(\mu_0 = 1)} = -\ln(1 - F_c) \frac{2}{\langle LAI \rangle} \tag{5}$$

[21] A formulation of the gap probability as a function of the Sun angle had been preliminarily explored by *Li et al.* [1995], though the solution provided here for multiple scattering is better suited for climate models.

2.3.2. Effective Values for the Optical Properties

[22] Once the effective LAI value is estimated, the diffusely transmitted and the backscattered fluxes associated with the Black Background contribution in (2) can be

Table 2. Variables Defining the Spectral Leaf and Soil Properties of the Structurally Heterogeneous Scenes

Variable Identification	Red Values	Near-Infrared Values
Leaf scatterer reflectance[a]	0.018	0.486
Leaf scatterer transmittance[a]	0.021	0.462
Trunk reflectance[b]	0.294	0.591
Soil reflectance[b]	0.173[c]	0.206[c] and 0.814[d]

[a]Using a bi-Lambertian scattering law.
[b]Using a Lambertian scattering law.
[c]Typical scenario conditions.
[d]Snow cover conditions simulated in the near-infrared.
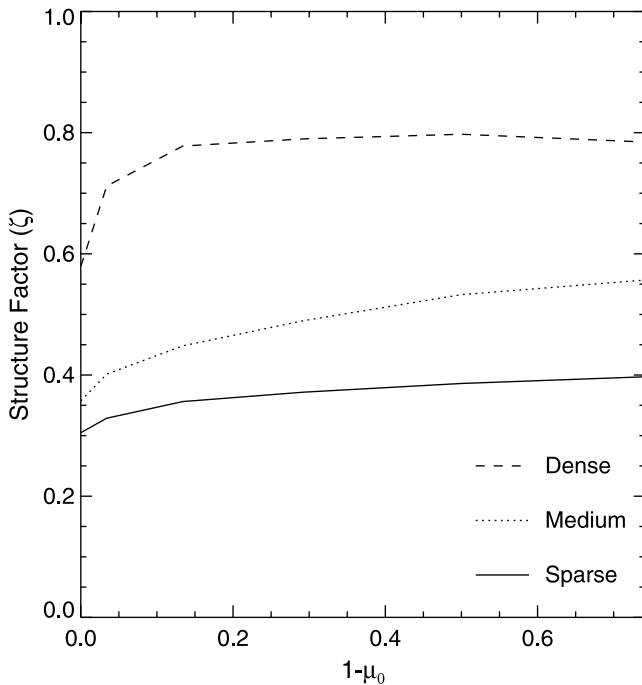
Figure 2. Variation of the structure factor as a function of the cosine of the Sun zenith angle $(1 - \mu_0)$, for the sparse, medium and dense scenarios described in Tables 1 and 2.

jointly used in an inversion mode to retrieve the effective reflectance $\widetilde{r_l}$ and transmittance $\widetilde{t_l}$ values of the scatterers [*Pinty et al.*, 2004, section 3.3.2]. Table 3 summarizes the results of estimating the effective reflectance $\widetilde{r_l}$ and transmittance $\widetilde{t_l}$ values of the scatterers resulting from the inversion of the scattered and diffusely transmitted fluxes delivered by two-stream solutions (B2) and (B3) to be discussed later in this paper (see also section 2.4), respectively, against the Raytran simulated results for the three heterogeneous scenarios described in Tables 1 and 2. It was also found that, for all practical purposes, the smooth dependency of $\widetilde{r_l}$ and $\widetilde{t_l}$ with respect to μ_0 can be neglected and the effective values were optimized for the $[0-75°]$ range in Sun zenith angles. Note that these effective values account implicitly for both the woody and the leaf elements of the vegetation canopies.

[23] As can be seen by comparing the results reported in Tables 2 and 3, the effective reflectance (transmittance) are increased (decreased) by a significant factor in the near-infrared domain with respect to the actual values assigned to the leaves in the 3-D scenarios. The effective single scattering albedo, $\omega_l = \widetilde{r_l} + \widetilde{t_l}$, is found to be about 10 to 20% smaller than the corresponding actual values in the near-infrared spectral domain. At this same wavelength, the correct estimates of the diffusely transmitted fluxes impose increasing the backward scattering regime yielding $\widetilde{r_l}/\widetilde{t_l}$ ratio much larger than unity [*Pinty et al.*, 2004, section 3.3.3].

2.4. Black Background Contribution

[24] The reflected and diffusely transmitted radiant fluxes associated with the Black Background contribution can be approximated by the classical two-stream solution of a radiative system where the state variables are $\widetilde{LAI}(\mu_0)/2$, $\widetilde{r_l}$ and $\widetilde{t_l}$. Formulations and applications of two-stream solu-

tions abound in the literature. For all practical purposes, the generic solutions proposed by, e.g., *Meador and Weaver* [1980, section 3] in the case of an atmospheric layer overlying a Black Background fulfills our needs. In the particular but reasonable case of leaves with all orientations of equal probabilities inside the tree crowns, yielding the 1/2 weighting factor of $\widetilde{LAI}(\mu_0)$, the set of the four γ coefficients required in the *Meador and Weaver*'s [1980] solutions were established and are given in Table 4 (see also Appendix A). Following *Meador and Weaver*'s [1980] terminology, γ_3 (γ_4) corresponds to the intercepted fraction of direct radiation scattered in the backward (forward) direction, i.e., creating a source term inside the medium, while γ_1 (γ_2) corresponds to the fraction of the scattered radiation which is redirected in the forward (backward) hemisphere. Adopting a spherical leaf angle distribution function greatly simplifies the formulation of the γ coefficients. The specific contributions to these coefficients that are due to the structure factor are embedded into the $\widetilde{r_l}$ and $\widetilde{t_l}$ values through the retrieval process described in *Pinty et al.* [2004, section 3.3.2]. In other words, the $\widetilde{r_l}$ and $\widetilde{t_l}$ values are optimized such that the complex dependency of the fraction of backward and forward scattered flux with respect to the structure factor at the domain resolution coupled with the leaf angle distribution function at the tree resolution, is accounted for. For the sake of completeness, Appendix A provides the sets of γ coefficients to be used in the *Meador and Weaver*'s [1980] two-stream formulation and applicable to the case of structurally homogeneous canopies composed of leaves exhibiting preferred orientations, i.e., spherical, planophile and erectophile.

[25] The set of γ coefficients given in Table 4 permits us to estimate the fraction of reflected and transmitted fluxes for the Black Background contribution. The lenghty analytical expressions for the reflected $R_{veg}^{Coll}(z_{toc}, \mu_0)$ and transmitted $T_{veg}^{Coll}(z_{bgd}, \mu_0)$ fluxes for all orders of scattering are the same as those given in *Meador and Weaver* [1980, equations (14) and (15)] and are duplicated in Appendix B for convenience.

[26] The reflected flux values associated with the first two orders of scattering (with respect to the external source of collimated radiation) in the vegetation layer only can straightforwardly be estimated by choosing the right set of γ coefficients as indicated in Table 4. Under conditions which are relevant for the vegetation canopy problem in the visible part of the spectrum, the corresponding analytical expressions for the DHR are as follows:

$$R_{veg}^{Coll1,2s}(z_{toc}, \mu_0) = R_{veg}^{1/2\infty}(z_{toc}, \mu_0)$$
$$\cdot \left[1 - \exp\left(-\frac{\widetilde{LAI}(\mu_0)}{2} \left(\frac{1}{\mu_0} + \gamma_1 \right) \right) \right] \quad (6)$$

Table 3. Effective Values of Leaf Optical Properties

Variable Identification	Scenario	Red[a]	Near-Infrared[a]
Scatterer reflectance $\widetilde{r_l}$	Sparse	0.017	0.639
	Medium	0.011	0.704
	Dense	0.017	0.801
Scatterer transmittance $\widetilde{t_l}$	Sparse	0.023	0.112
	Medium	0.024	0.074
	Dense	0.011	0.008

[a]From an inversion of the Black Background two-stream solutions (B2) and (B3) over the range $[0-75°]$ in Sun zenith angles.

Table 4. Expressions for the γ Coefficients for the Case of Vegetation Required in the Two-Stream Solution Proposed by *Meador and Weaver* [1980, equations (14) and (15)] with $\omega_l^{\mathrm{a}} = (\widetilde{r_l} + \widetilde{t_l})$ and $\delta_l^{\mathrm{a}} = (\widetilde{r_l} - \widetilde{t_l})$

Scattering Order	γ_1	γ_2	γ_3	γ_4
First[b]	2	0	$2\left[\frac{\omega_l}{4} + \mu_0 \frac{\delta_l}{6}\right]/\omega_l$	$2\left[\frac{\omega_l}{4} - \mu_0 \frac{\delta_l}{6}\right]/\omega_l$
First and second[b]	$2[1 - \frac{\omega_l}{2} + \frac{\delta_l}{6}]$	0	idem	idem
All	idem	$2[\frac{\omega_l}{2} + \frac{\delta_l}{6}]$	idem	idem

[a]Using the inversion scheme described in section 2.3.2.
[b]With respect to the external collimated source of radiation.

where $R_{veg}^{1/2\infty}$ denotes the flux reflected by a radiatively semi-infinite vegetation canopy given by the following expression when accounting for the first two orders of anisotropic scattering:

$$R_{veg}^{1/2\infty}(z_{toc}, \mu_0) = \frac{\omega_l \gamma_3}{1 + \gamma_1 \mu_0} \qquad (7)$$

[27] Effective LAI values are generally smaller than the corresponding true values in 3-D scenarios, though they can occasionally be larger, especially for low LAI canopies, due to the contribution of stems. Note that requiring the use of effective LAI values implies a reduction in the frequency of occurrence of optically deep canopies.

[28] Following that same two-stream approach, the associated total (direct plus diffuse) transmission factor is given by:

$$T_{veg}^{Coll1,2s}(z_{bgd}, \mu_0) = \exp\left(-\widetilde{LAI}(\mu_0)/2\mu_0\right) \left\{ 1 - \frac{\omega_l \gamma_4}{1 - \gamma_1 \mu_0} \right.$$
$$\left. \cdot \left[1 - \exp\left(\frac{\widetilde{LAI}(\mu_0)}{2}\left(\frac{1}{\mu_0} - \gamma_1\right)\right)\right]\right\}$$
$$\gamma_1 \mu_0 \neq 1 \qquad (8)$$

using the γ coefficient values indicated in the first two rows in Table 4. Since the fraction of absorbed radiation, $A_{veg}^{Coll1,2s}(z_{bgd}, \mu_0)$ is simply given by the closure of the radiation balance equation for a black background condition, i.e., $A_{veg}^{Coll1,2s} = 1 - (R_{veg}^{Coll1,2s} + T_{veg}^{Coll1,2s})$, it can be expressed as:

$$A_{veg}^{Coll1,2s}(\mu_0) = \left[1 - \exp\left(-\widetilde{LAI}(\mu_0)/2\mu_0\right)\right]$$
$$+ \omega_l \left[f_1\left(\widetilde{LAI}(\mu_0), \mu_0, \gamma_1, \gamma_4\right)\right.$$
$$\left. - f_2\left(\widetilde{LAI}(\mu_0), \mu_0, \gamma_1, \gamma_3\right)\right] \qquad (9)$$

where f_1 (f_2) represents the contribution due to the diffuse downward (upward) transmitted scattered flux. These are complex functions of the variables mentioned in parentheses which can be straightforwardly derived from (6) and (8).

[29] Equation (9) suggests that the fraction of the direct radiation absorbed by the Black Background contribution in the red spectral domain is strongly dominated by the first term on the right hand side which corresponds to the fraction of intercepted radiation. Indeed, the second term on the right hand side of (9) is weighted by the single scattering albedo which takes on small values since leaves are efficiently absorbing short wavelength radiation.

[30] The accuracy available from the two-stream solutions proposed by *Meador and Weaver* [1980, equations (14) and

(15)] (see also (B2) and (B3)) was evaluated against a Monte-Carlo method for a wide set of variable values spanning a range relevant for the vegetation case (see Table 5). Extreme values of the ratio $\widetilde{r_l}/\widetilde{t_l}$ were added to test the performance of the two-stream solutions under physically stringent conditions. Note that the proposed set of two-stream solutions are designed for addressing anisotropic leaf scattering properties which is a prerequisite given the typical range of $\widetilde{r_l}/\widetilde{t_l}$ given in Table 3. Since the direct transmission factor is represented exactly, Figure 3 displays results obtained for the diffuse component only, that is $t_{veg}^{Coll}(z_{bgd}, \mu_0) = T_{veg}^{Coll}(z_{bgd}, \mu_0) - \exp(-\widetilde{LAI}(\mu_0)/2\mu_0)$. This figure illustrates the good performance of the two-stream solutions, i.e., limited bias and scatter around the one to one line, in the red (significant absorption) and near-infrared (significant contribution due to multiple scattering) spectral domains, for both R_{veg}^{Coll} and t_{veg}^{Coll}. It is noteworthy that the relative contribution due to the direct component, $\exp(-\widetilde{LAI}(\mu_0)/2\mu_0)$, with respect to the total, is large enough under canopy conditions yielding the largest discrepancies displayed on Figure 3, such that the overall agreement between the total directional transmission factors is very good, for all practical purposes.

[31] The relative contributions due to the first two orders of scattering with respect to the full solution are shown in Figure 4 for both the reflected and diffusely transmitted radiant fluxes. In the red spectral domain (top panel), strong leaf absorption translates into a small value of the single scattering albedo ω_l and, thus, the solution given by considering the first two orders of scattering only, constitutes a very good approximation of the full solution. However, in the near-infrared spectral domain, multiple scattering is significant. Large values of $\widetilde{LAI}(\mu_0)$ yield the worst case scenarios depending on the back/forward scattering efficiency that is, the ratio $\widetilde{r_l}/\widetilde{t_l}$ given in Table 5: $\widetilde{r_l}/\widetilde{t_l} < 1$ ($\widetilde{r_l}/\widetilde{t_l} > 1$) favors forward (backward) scattering and the first two orders of scattering may only account for about 50% (70%) of the total in the worst case scenarios. The opposite situation holds when considering the diffuse component of the total transmission factor. The condition

Table 5. Variable Values Adopted to Evaluate the Accuracy of the Two-Stream Based Solutions Valid for the Structurally Homogeneous Case

Variable Identification	Values
Sun zenith angle	0, 30, 60 and 80°
$\widetilde{LAI}$	0.5, 1, 3 and 6 (m²/m²)
$\widetilde{r_l}/\widetilde{t_l}$	0.1, 0.2, 0.5, 1, 2, 5 and 10
$\omega_l = \widetilde{r_l} + \widetilde{t_l}$	from 0.025 to 0.25 in steps of 0.025 (red domain) from 0.7 to 0.95 in steps of 0.05 (near-infrared domain)
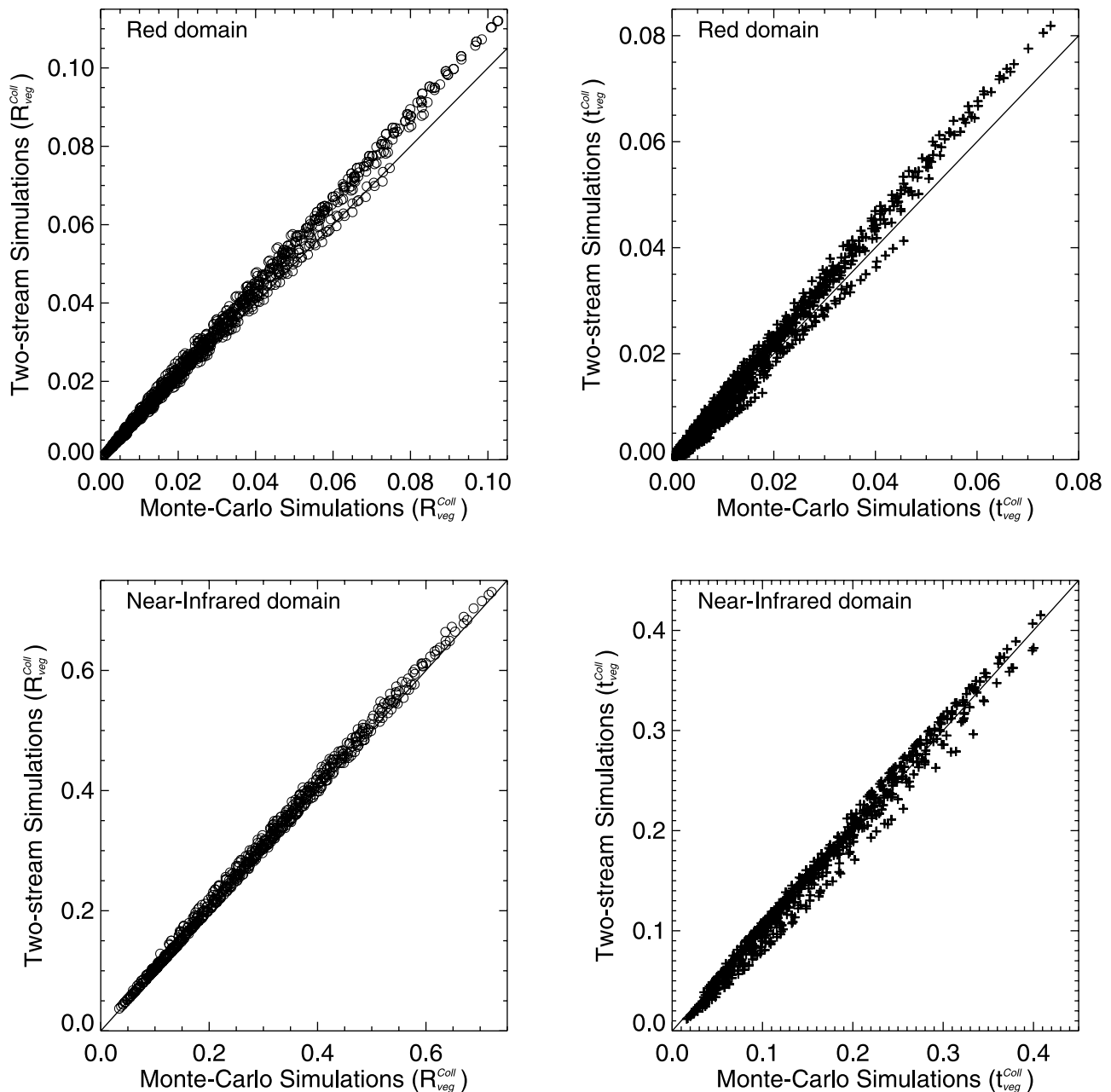
Figure 3. Comparison between the reflected R_{veg}^{Coll} (left panels) and diffusely transmitted t_{veg}^{Coll} (right panels) radiant fluxes estimated using the full solutions resulting from a two-stream approximation, (B2) and (B3), respectively, against those simulated with a Monte-Carlo approach. The top (bottom) panels correspond to typical conditions occurring in the red (near-infrared) spectral domain. The evaluation is performed for all cases included in Table 5.

$\widetilde{r_l}/\widetilde{t_l} > 1$, that translates into canopies optically deeper than for isotropic scattering, is more likely to happen in the near-infrared spectral domain [*Pinty et al.*, 2004].

[32] The expressions given by (6) and (7) differ in many respects from those sometimes implemented, for instance, in the Common Land Model (CLM) albedo scheme [e.g., *Zhou et al.*, 2003] to represent this Black Background contribution. For instance, the CLM scheme prescribes the values for the optically deep canopy albedo, $R_{veg}^{1/2\infty}(z_{toc}, \mu_0)$, that are not, as suggested by (7), (1) dependent on the Sun zenith angle and (2) driven by leaf scattering properties

which are themselves assigned fixed values in the CLM ($\omega_l =$ 0.15 and 0.85 for the red and near-infrared spectral domains, respectively). There is thus some inconsistency in the CLM to impose fixed values for the leaf properties while allowing the albedo for optically deep canopies to change as a function of the biome type. Moreover, the bracketed term in (6), which represents the scattering contribution due to finite canopy optical thickness, also differs from the corresponding one sometimes adopted in the CLM albedo scheme. Indeed, following this CLM type of implementation [e.g., *Zhou et al.*, 2003, equation (12)] and using (7), (6) can
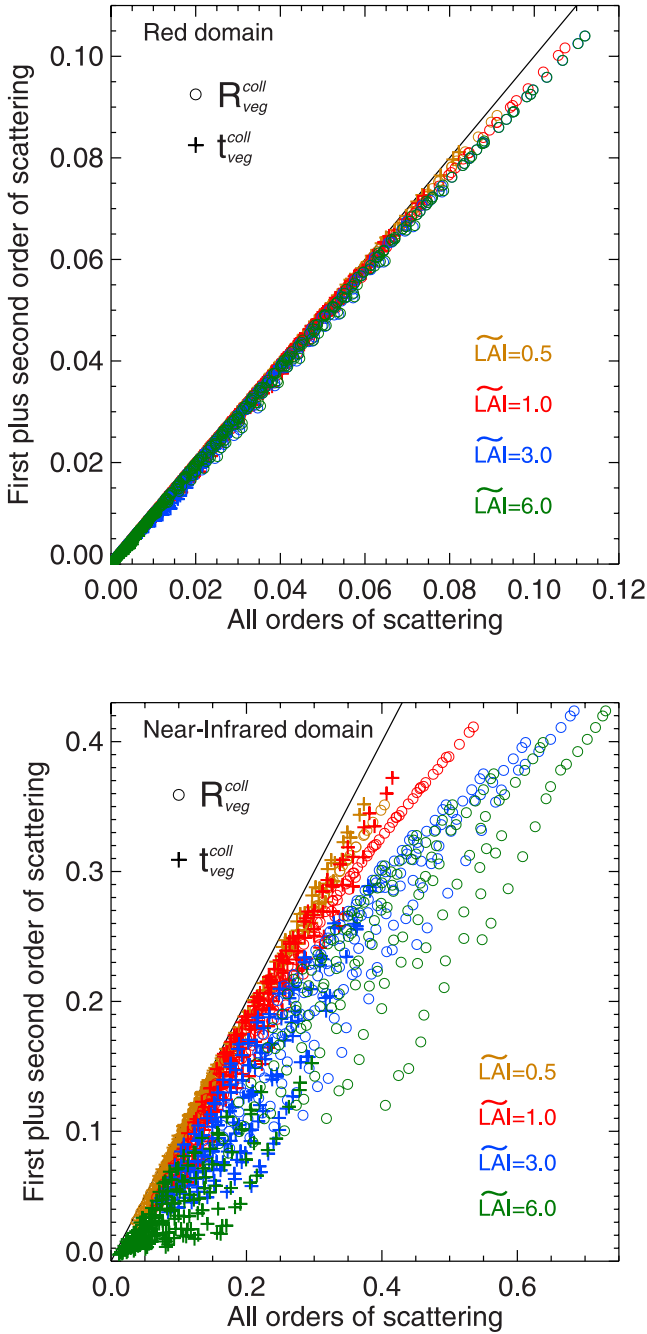
Figure 4. Comparison between the reflected and diffusely transmitted radiant fluxes estimated using the first two orders of scattering only, $R_{veg}^{Coll1,2s}$ from (6) and $t_{veg}^{Coll1,2s}$ from (8), respectively, against those obtained from the full solutions, R_{veg}^{Coll} from (B2) and t_{veg}^{Coll} from (B3). The top (bottom) panel corresponds to typical conditions occurring in the red (near-infrared) spectral domain. The evaluation is performed for all cases included in Table 5.

be rewritten as:

$$R_{veg}^{Coll1,2s}(z_{toc}, \mu_0) = R_{veg}^{1/2\infty}(z_{toc}, \mu_0) \left[1 - \exp\left(-\frac{\widetilde{LAI}(\mu_0)}{2} \right. \right.$$
$$\left. \left. \cdot \left(\frac{\omega_l \gamma_3}{\mu_0 R_{veg}^{1/2\infty}(z_{toc}, \mu_0)} \right) \right) \right] \quad (10)$$

[33] In the limit of isotropic single scattering assumption, (10) differs from the CLM formula by a factor of 2 in the argument of the exponential. It thus looks like the contribution to the total albedo due to the Black Background component is sytematically overestimated by the CLM except for optically deep canopies, unless compensation exists somewhere else, e.g., through prescribing ad hoc values to the other variable entering the model albedo calculations.

2.5. Black Canopy Contribution

[34] Following *Pinty et al.* [2004], the BRF field associated with the Black Canopy contribution can be expressed as:

$$\rho_{bgd}^{UnColl}(z_{toc}, \Omega, \Omega_0) = \rho_{bgd}(z_{bgd}, \Omega, \Omega_0)$$
$$\cdot T_{veg}^{\downarrow UnColl}(z_{bgd}, \Omega_0) \, T_{veg}^{\uparrow UnColl}(z_{toc}, \Omega) \quad (11)$$

where the angular dependency of $\widetilde{LAI}$ has been omitted:

$$T_{veg}^{\downarrow UnColl}(z_{bgd}, \Omega_0) = \exp\left(-\widetilde{LAI}/2\mu_0 \right)$$
$$T_{veg}^{\uparrow UnColl}(z_{toc}, \Omega) = \exp\left(-\widetilde{LAI}/2\mu \right) \quad (12)$$

[35] Note that (12) and further equations use the azimuthal average of the uncollided upward and downward direct transmission functions. These expressions also neglect specific features arising from actual 1-D discrete and 3-D situations such as the enhanced backscattering effects known as the hot spot phenomenon. At this stage, the latter contribution to the total albedo is not accounted for since the impact of this specific effect is considered negligible. Thus the corresponding contribution to the total DHR, $R_{bgd}^{UnColl}(z_{toc}, \Omega_0)$, in the case of a background which BHR (or white sky albedo) is noted R_{bgd}, becomes:

$$R_{bgd}^{UnColl}(z_{toc}, \mu_0) = R_{bgd} \exp\left(-\widetilde{LAI}/2\mu_0 \right) \overline{T_{veg}^{UnColl}}(z_{toc}) \quad (13)$$

with

$$\overline{T_{veg}^{UnColl}}(z_{toc}) = 2 \int_0^1 \exp\left(-\widetilde{LAI}(\mu)/2\mu \right) \mu \, d\mu \quad (14)$$

[36] It is possible to solve (14) if one assumes the functional dependency of $\widetilde{LAI}$ on μ. Using (4) for expressing $\widetilde{LAI}(\mu)$ yields the following approximation of (14):

$$\overline{T_{veg}^{UnColl}}(z_{toc}) \approx 2 \int_0^1 \exp\left(-\widetilde{LAI}^\star/2\mu \right) \mu \, d\mu \quad (15)$$

where $\widetilde{LAI}$ is the effective LAI value satisfying (4) at $\mu = 0.5$. Accordingly, the solution to (15) is given by the following analytical expression:

$$\overline{T_{veg}^{UnColl}}(z_{toc}) = \exp\left(-\widetilde{LAI}^\star/2 \right) \left[1 - \widetilde{LAI}^\star/2 + \left(\widetilde{LAI}^\star/2 \right)^2 \right.$$
$$\left. \times \exp\left(\widetilde{LAI}^\star/2 \right) \Gamma\left(0, \widetilde{LAI}^\star/2 \right) \right] \quad (16)$$
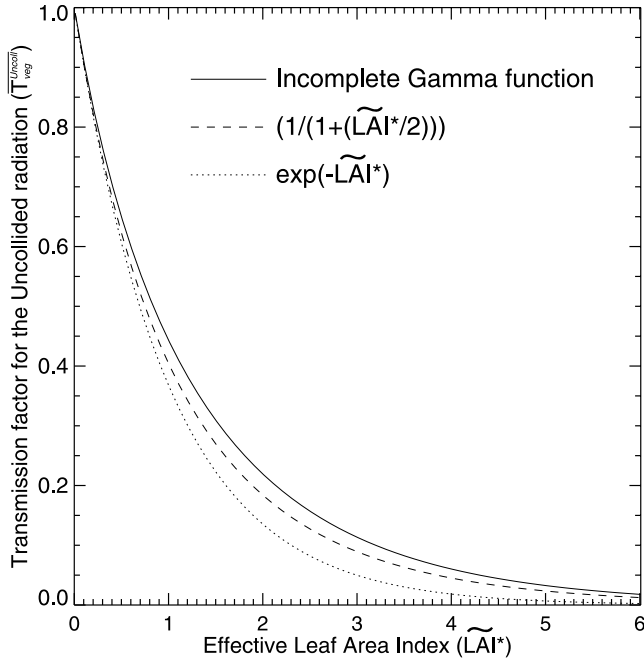
Figure 5. Comparison between results obtained using equations (16), (18), and (19), respectively, entering the estimation of the directional Hemispherical transmission factor for the upward travelling uncollided radiation.

where

$$\mathbf{\Gamma}\left(0, \widetilde{LAI^\star}/2\right) = \int_{\widetilde{LAI^\star}/2}^{\infty} t^{-1} \exp(-t)\, dt \qquad (17)$$

is the incomplete Gamma function that can be evaluated accurately using a continued fraction development for any value of $\widetilde{LAI}/2$ [*Abramowitz and Stegun*, 1970, p. 263, equation (6.5.31)]. It is worthwhile to note that for typical range of values of $\widetilde{LAI}/2$, i.e., less than 5, $\overline{T_{veg}^{UnColl}}(z_{toc})$ can be approximated by:

$$\overline{T_{veg}^{UnColl}}(z_{toc}) \approx \exp\left(-\widetilde{LAI^\star}/2\right)\left(\frac{1}{1 + \widetilde{LAI^\star}/2}\right) \qquad (18)$$

and, thus, the power-law of attenuation (18) reduces to the classical exponential attenuation under conditions where $\widetilde{LAI^\star}/2$ or $\zeta^\star$ is small enough, yielding:

$$\overline{T_{veg}^{UnColl}}(z_{toc}) \approx \exp\left(-\widetilde{LAI^\star}\right) \approx \exp(-\langle LAI \rangle \zeta^\star)$$

$$\widetilde{LAI^\star} \to 0 \qquad (19)$$

[37] The $\zeta^\star$ factor can be further interpreted as an hemispherical structure factor expressing the effects due to the internal variability of the leaf area density inside the domain resulting from 3-D vegetation architecture. One may anticipate that this hemispherical factor can be linked to statistical descriptors of the domain-averaged heterogeneity such as, for instance, the first order structure function, or "Hurst", exponent of canopy density and

height fields [*Widlowski et al.*, 2001b] and/or tree scale statistics such as the ratio between average tree density and the mean nearest tree distance [*Widlowski et al.*, 2004] (see Table 1) and/or any other appropriate indicator as suggested by *Knyazikhin et al.* [1998a].

[38] By definition the structure factor is equal to unity only for a structurally homogeneous turbid plane parallel medium and, in this case, (13), $R_{bgd}^{UnColl}(z_{toc}, \mu_0)$ reduces to:

$$R_{bgd}^{UnColl}(z_{toc}, \mu_0) = R_{bgd}\, \exp\left(-\widetilde{LAI}/2\mu_0\right) \exp\left(-\widetilde{LAI^\star}\right)$$

$$\widetilde{LAI} \to 0 \qquad (20)$$

[39] Equation (20) is identical to the solution implemented, for instance, in the Common Land Model (CLM) albedo scheme [e.g., *Zhou et al.*, 2003] to represent the contribution to surface albedo that is due to the background underneath the vegetation layer. This formulation is thus valid for optically thin vegetation layers.

[40] Figure 5 shows a comparison between results from (16), (18), and (19). It suggests that, for all practical purposes, (18) offers a good compromise between accuracy and computational cost for both small and large LAI values, i.e., it preserves the deviation from the exponential decay and is easy to estimate. Note also that, under conditions where $\widetilde{LAI}$ takes intermediate values ($\widetilde{LAI} \approx 1$), (19) can significantly underestimate the directly transmitted flux compared to (18) and, in doing so, degrade the accuracy of the absorbed flux. The accuracy estimation of $\overline{T_{veg}^{UnColl}}(z_{toc})$ is, however, largely preserved by weighting the argument of the exponential in (19) with an empirical factor equal to 0.705. Alternatively, (18) can be made to fit better the exact solution expressed by (15) simply by replacing the 0.5 factor by 0.45, both in the exponential and the denominator.

2.6. Coupled Canopy-Background Contribution

[41] Following the approach proposed by *Pinty et al.* [2004], and adopting a turbid medium representation, the contribution to the BRF field due to the multiple interactions between the background and the vegetation layer can be written as:

$$\rho_{bgd}^{Coll}(z_{toc}, \Omega, \Omega_0) = \rho_{bgd}(z_{bgd}, \Omega, \Omega_0) \left[\breve{\rho}_{bgd\mathbf{1}}^{Coll}(z_{toc}, \Omega, \Omega_0)\right.$$
$$\left. + \breve{\rho}_{bgd\mathbf{n}}^{Coll}(z_{toc}, \Omega, \Omega_0)\right] \qquad (21)$$

where the first bracketed term $\breve{\rho}_{bgd\mathbf{1}}^{Coll}(z_{toc}, \Omega, \Omega_0)$ represents the contribution to the angular field of the BRF due to the radiation singly collided by the background before or after being scattered at least once by the vegetation layer. The second bracketed term, $\breve{\rho}_{bgd\mathbf{n}}^{Coll}(z_{toc}, \Omega, \Omega_0)$ represents the additional contribution involving multiple canopy-background interactions. These contributions to the reflected radiant flux can thus be formally expressed as:

$$R_{bgd}^{Coll}(z_{toc}, \mu_0) = R_{bgd}\left[\breve{R}_{bgd\mathbf{1}}^{Coll}(z_{toc}, \mu_0) + \breve{R}_{bgd\mathbf{n}}^{Coll}(z_{toc}, \mu_0)\right] \qquad (22)$$

where $\breve{R}_{bgd\mathbf{1}}^{Coll}$ involves both the diffuse downward and upward transmission factors (estimated with no contamina-

tion by the background). Its contribution is formally given by:

$$
\begin{aligned}
\breve{R}^{Coll}_{bgd\,1}(z_{toc}, \mu_0) = {} & \exp\left(-\widetilde{LAI}/2\mu_0\right) \times 2 \int_0^1 t^{Coll}_{veg}(z_{toc}, \mu)\,\mu\,d\mu \\
& + t^{Coll}_{veg}(z_{bgd}, \mu_0) \times 2 \int_0^1 \exp\left(-\widetilde{LAI}/2\mu\right)\mu\,d\mu \\
& + t^{Coll}_{veg}(z_{bgd}, \mu_0) \times 2 \int_0^1 t^{Coll}_{veg}(z_{toc}, \mu)\,\mu\,d\mu
\end{aligned}
$$
(23)

where $t^{Coll}_{veg}(z_{ref}, \mu_x)$ is the diffuse part of the directional hemispherical transmission factor. Equation (23) can be equivalently estimated with the following expression:

$$
\begin{aligned}
\breve{R}^{Coll}_{bgd\,1}(z_{toc}, \mu_0) = {} & T^{Coll}_{veg}(z_{bgd}, \mu_0)\,\overline{T^{Coll}_{veg}}(z_{toc}) \\
& - \exp\left(-\widetilde{LAI}/2\mu_0\right)\overline{T^{UnColl}_{veg}}(z_{toc})
\end{aligned}
$$
(24)

[42] Exact and approximate solutions for $\overline{T^{UnColl}_{veg}}$ were established in section 2.5. $\overline{T^{Coll}_{veg}}(z_{toc})$ is the bi-hemispherical transmission factor for total upward radiation assuming an isotropic source at the bottom of the canopy, that is:

$$
\overline{T^{Coll}_{veg}}(z_{toc}) = 2 \int_0^1 T^{Coll}_{veg}(z_{bgd}, \mu')\,\mu'\,d\mu'
$$
(25)

[43] This quantity can be estimated accurately by the solutions of the two-stream approximations derived for an isotropic source of illumination (see Appendix B). Note that for single scattering conditions by the homogeneous vegetation layer, $\overline{R^{Coll1s}_{veg}} \rightarrow \gamma_2/4$ when the vegetation layer becomes optically deep. This approximation was already established by *Dickinson* [1983, equation (2.15)] and further served as a baseline for assigning typical values to optically deep vegetation canopies in the CLM.

[44] Following *Pinty et al.* [2004], the additional contribution involving multiple canopy-background interactions in (22) can be written as:

$$
\breve{R}^{Coll}_{bgd\,\mathbf{n}}(z_{toc}, \mu_0) = \overline{T^{Coll}_{veg}}(z_{toc})\,S^{Coll}_{bgd\,\mathbf{n}}(z_{bgd}, \mu_0)
$$
(26)

[45] The term $S^{Coll}_{bgd\mathbf{n}}(z_{bgd}, \mu_0)$ in (26) represents the source term at the background level due to multiple scattering between the background and the vegetation layer. It can itself be approximated as:

$$
S^{Coll}_{bgd\,\mathbf{n}}(z_{bgd}, \mu_0) \approx T^{Coll}_{veg}(z_{bgd}, \mu_0)\,R_{bgd}\,\frac{\overline{R^{Coll}_{veg}}(z_{toc})}{1 - R_{bgd}\,\overline{R^{Coll}_{veg}}(z_{toc})}
$$
(27)

where $\overline{R^{Coll}_{veg}}(z_{toc})$ can be estimated accurately by the solutions of the two-stream approximations derived for an isotropic source of illumination (see Appendix B).

2.7. Summary of the Proposed Radiation Scheme

[46] This section summarizes the results established so far and highlights some of the simplifications implied when considering only the first two orders of scattering within the vegetation layer.

2.7.1. Radiant Fluxes Associated With Direct Illumination

[47] According to (2) and developments proposed in sections 2.4, 2.5, and 2.6, the surface albedo of a radiatively

independent volume containing either 1-D or 3-D vegetation canopies can be formally written as:

$$
\begin{aligned}
R^{total}_{coupled}(z_{toc}, \mu_0) = {} & R^{Coll}_{veg}\left(z_{toc}, \mu_0; \widetilde{LAI}(\mu_0)/2, \widetilde{r}_l, \widetilde{t}_l\right) \\
& + R_{bgd}\Bigg\{ \overline{T^{UnColl}_{veg}}\left(z_{toc}; \widetilde{LAI}^\star/2, \widetilde{r}_l, \widetilde{t}_l\right) \\
& \cdot \exp\left(-\widetilde{LAI}(\mu_0)/2\mu_0\right) \\
& + \Big[\breve{R}^{Coll}_{bgd\,1}\left(z_{toc}, \mu_0; \widetilde{LAI}(\mu_0)/2, \widetilde{LAI}^\star, \widetilde{r}_l, \widetilde{t}_l\right) \\
& + \breve{R}^{Coll}_{bgd\,\mathbf{n}}\left(z_{toc}, \mu_0; \widetilde{LAI}(\mu_0)/2, \widetilde{LAI}^\star, \widetilde{r}_l, \widetilde{t}_l, R_{bgd}\right) \Big] \Bigg\}
\end{aligned}
$$
(28)

[48] Similarly, the domain-averaged total transmission factor associated with this 3-D vegetation canopy is written as:

$$
\begin{aligned}
T^{total}_{coupled}(z_{bgd}, \mu_0) = {} & T^{Coll}_{veg}\left(z_{bgd}, \mu_0; \widetilde{LAI}(\mu_0)/2, \widetilde{r}_l, \widetilde{t}_l\right) \\
& + S^{Coll}_{bgd\,\mathbf{n}}\left(z_{bgd}, \mu_0; \widetilde{LAI}^\star, \widetilde{r}_l, \widetilde{t}_l, R_{bgd}\right)
\end{aligned}
$$
(29)

and the corresponding absorbed flux, derived from the radiation balance equation for a non-black background, is expressed as (with omission of the state variables):

$$
\begin{aligned}
A^{total}_{coupled}(\mu_0) = {} & A^{Coll}_{veg}(\mu_0) + R_{bgd}\Bigg\{ T^{Coll}_{veg}(z_{toc}, \mu_0) \\
& - \Big[\overline{T^{UnColl}_{veg}}(z_{bgd})\,\exp\left(-\widetilde{LAI}(\mu_0)/2\mu_0\right) \\
& + \breve{R}^{Coll}_{bgd\,1}(z_{toc}, \mu_0) + \breve{R}^{Coll}_{bgd\,\mathbf{n}}(z_{toc}, \mu_0) \Big] \Bigg\} \\
& + S^{Coll}_{bgd\,\mathbf{n}}(z_{bgd}, \mu_0)\left[R_{bgd} - 1\right]
\end{aligned}
$$
(30)

where, depending on the desired accuracy, the Black Background contribution, R^{Coll}_{veg}, T^{Coll}_{veg} and A^{Coll}_{veg}, can be estimated using one of the proposed two-stream solutions, i.e., (B2) or (6) and (B3) or (8). The transmission factor $\overline{T^{UnColl}_{veg}}$ can be evaluated either with (16), (18) or (19), while $\breve{R}^{Coll}_{bgd\,1}$ and $\breve{R}^{Coll}_{bgd\mathbf{n}}$ are approximated using (24) and (26), respectively. The estimate of the latter two contributions can as well benefit from the simplified formulations proposed in Appendix B.

[49] It is noteworthy that in the cases where the multiple scattering is limited, e.g., low $\widetilde{LAI}$ and/or in the visible part of the solar spectrum where ω_l takes on small values, for large Sun zenith angles, the estimation of the radiant fluxes from (28), (29), and (30) is greatly simplified. For instance, in the single scattering limit with respect to the coupled vegetation-background system, the solution for $R^{total}_{coupled}$ is given by the first two terms in (28) only. Under these same scattering conditions, the fraction of total transmitted is equal to $\exp(-\widetilde{LAI}(\mu_0)/2\mu_0)$, leading to the following simple expression for the absorbed flux, from the closure of the radiation balance equation for the coupled vegetation-background system, i.e., $A^{1s}_{coupled} = 1 - (R^{1s}_{coupled} + T^{1s}_{coupled}) + R_{bgd} \times T^{1s}_{coupled}$:

$$
A^{1s}_{coupled}(\mu_0) \approx \left(1 - \exp\left(-\widetilde{LAI}(\mu_0)/2\mu_0\right)\right) + \delta_{A^{1s}_{coupled}}
$$
(31)

where the first term, on the right hand side of the equation, corresponds to the fraction of intercepted direct radiation and $\delta_{A_{coupled}^{1s}}$ accounts for all the remaining effects, that is:

$$
\begin{aligned}
\delta_{A_{coupled}^{1s}}(\mu_0) = {} & R_{bgd} \exp\left(-\widetilde{LAI}(\mu_0)/2\mu_0\right)\left(1 - \overline{T_{veg}^{UnColl}}\right) \\
& - R_{veg}^{Coll1s}(z_{toc}, \mu_0)
\end{aligned}
\tag{32}
$$

[50] $\delta_{A_{coupled}^{1s}}$ is thus a function expressing the balance between the contributions due to the fraction of upscattered flux at the bottom of the canopy (positive contribution), and the fraction of upscattered flux at the top of the canopy (negative contribution), that is the albedo of the Black Background contribution in the limit of single scattering. The former is logically given by the product of the isotropic source term illuminating the vegetation canopy from below, i.e., $R_{bgd} \exp(-\widetilde{LAI}(\mu_0)/2\mu_0)$, and the intercepted fraction over the entire upward hemisphere, i.e., $(1 - \overline{T_{veg}^{UnColl}})$.

[51] Given the order of magnitude of the two terms on the right hand side of (32), one may anticipate that the contribution due to the isotropic source of radiation at the bottom of the canopy largely offsets the one due to the canopy albedo. Indeed, for low (high) vegetation density conditions, the fraction of absorbed flux is rather small (large) so that the deviation from the intercepted flux as expressed by (32) remains limited, i.e., less than +0.05, provided the background brightness takes on normal values. The worst case scenario occurs when considering intermediate range of LAI/density conditions, especially in the red spectral region of the spectrum where canopy albedo is small due to the significant leaf absorption.

[52] The accuracy and relevance of the solution derived when accounting for the first orders of scattering by the coupled Canopy-Background system will be evaluated in section 3 against full solutions estimated with realistic 3-D scenarios.

[53] Equations (28), (29), and (30) constitute one of the few sets of formulae that can be adopted to represent the DHR, the transmission and thus the absorption factors contributing to the parameterization of the radiant fluxes with respect to a direct source of illumination. These specific formulae have the advantage to separate the scattering contributions due to the background (including the first order from the rest) from those invoking the vegetation layer itself.

2.7.2. Radiant Fluxes Associated With Diffuse Illumination

[54] The $BHR_{iso}(z_{toc})$ contribution to (1) is deduced from the corresponding DHR (z_{toc}, μ_0), namely $R_{coupled}^{total}$, by replacing, in (28), the directional hemispherical reflectance and transmission factors for downward radiation by their corresponding bi-hemispherical values. Since the vegetation layer is assumed to be vertically uniform, the latter are the same for both the upward and downward directions. The following equation is thus obtained:

$$
\begin{aligned}
\overline{R_{coupled}^{total}}(z_{toc}) = {} & \overline{R_{veg}^{Coll}}\left(z_{toc}; \widetilde{LAI}^{\star}, \widetilde{r}_l, \widetilde{t}_l\right) \\
& + R_{bgd} \frac{\overline{T_{veg}^{Coll}}^{\,2}\left(z_{toc}; \widetilde{LAI}^{\star}, \widetilde{r}_l, \widetilde{t}_l\right)}{1 - R_{bgd}\,\overline{R_{veg}^{Coll}}\left(z_{toc}; \widetilde{LAI}^{\star}, \widetilde{r}_l, \widetilde{t}_l\right)}
\end{aligned}
\tag{33}
$$

[55] In (33), the bi-hemispherical reflectance $\overline{R_{veg}^{Coll}}$ and the transmission factor $\overline{T_{veg}^{Coll}}$ can be estimated following the

procedures described in Appendix B. The fraction of absorbed radiation under diffuse sky illumination can thus be approximated by the following expression in the limit of the single scattering regime:

$$
\overline{A_{coupled}^{1s}} \approx \left(1 - \overline{T_{veg}^{UnColl}}\right) + \overline{\delta_{A_{coupled}^{1s}}}
\tag{34}
$$

where the first term on the right hand side of the equation corresponds to the fraction of intercepted diffuse radiation and $\overline{\delta_{A_{coupled}^{1s}}}$ is given by:

$$
\overline{\delta_{A_{coupled}^{1s}}} = R_{bgd}\,\overline{T_{veg}^{UnColl}}\left(1 - \overline{T_{veg}^{UnColl}}\right) - \overline{R_{veg}^{Coll1s}}(z_{toc})
\tag{35}
$$

[56] As discussed previously, for highly absorbing conditions such as those prevailing in the visible part of the spectral domain, and excluding exceptionally bright background conditions, e.g., snow covered background, (34) and (35) indicate that the fraction of diffuse radiation intercepted by the canopy controls the major part of the absorbed fraction.

[57] As can readily be seen by comparing the formulations obtained in the limit of single scattering with respect to direct and diffuse illumination, (31) and (34) respectively, the vegetation canopy layer intercepts and thus absorbs more (less) efficiently the diffuse sky illumination than the direct one for low (high) Sun zenith angle values. This effect is especially enhanced in the case of 3-D structurally heterogeneous media since, in addition to the μ_0 effect, $\widetilde{LAI}^{\star} > \widetilde{LAI}$ for low Sun zenith angle values. The diffuse sky radiation therefore tends to smooth the angular dependency of the absorbed flux with respect to the Sun zenith angle.

3. Accuracy of the Proposed Two-Stream Solutions

[58] This section investigates in detail the performance of the two-stream solutions for simulating jointly the scattered, transmitted and absorbed radiant fluxes that occur in realistic 3-D situations. To this end, the radiation transfer regimes of the three 3-D scenes presented in Tables 1 and 2 were calculated using the Raytran ray tracing Monte-Carlo model [*Govaerts and Verstraete*, 1998] and the three separate contributions, namely those due to the Black Background, the Black Canopy, and the multiple scattering between the background and the canopy, respectively, were estimated separately as proposed in (2).

[59] Figure 6 shows the relative contribution of each term to the total DHRs as a function of Sun zenith angle. The evaluation of the various relative contributions to the total signal helps better assessing the level of assumptions, e.g., using solutions derived in the limit of single scattering and/or small LAI conditions, that can be adopted for an accurate simulations of the three radiant fluxes. For all practical purposes, the scenarios implementing the difficult case of a background covered by snow is the most demanding in terms of accuracy of the Black Canopy and coupled Canopy-Background contributions.

[60] Figure 7 illustrates the performance and errors associated with the various two-stream based solutions established for the DHR component of the surface albedo in the
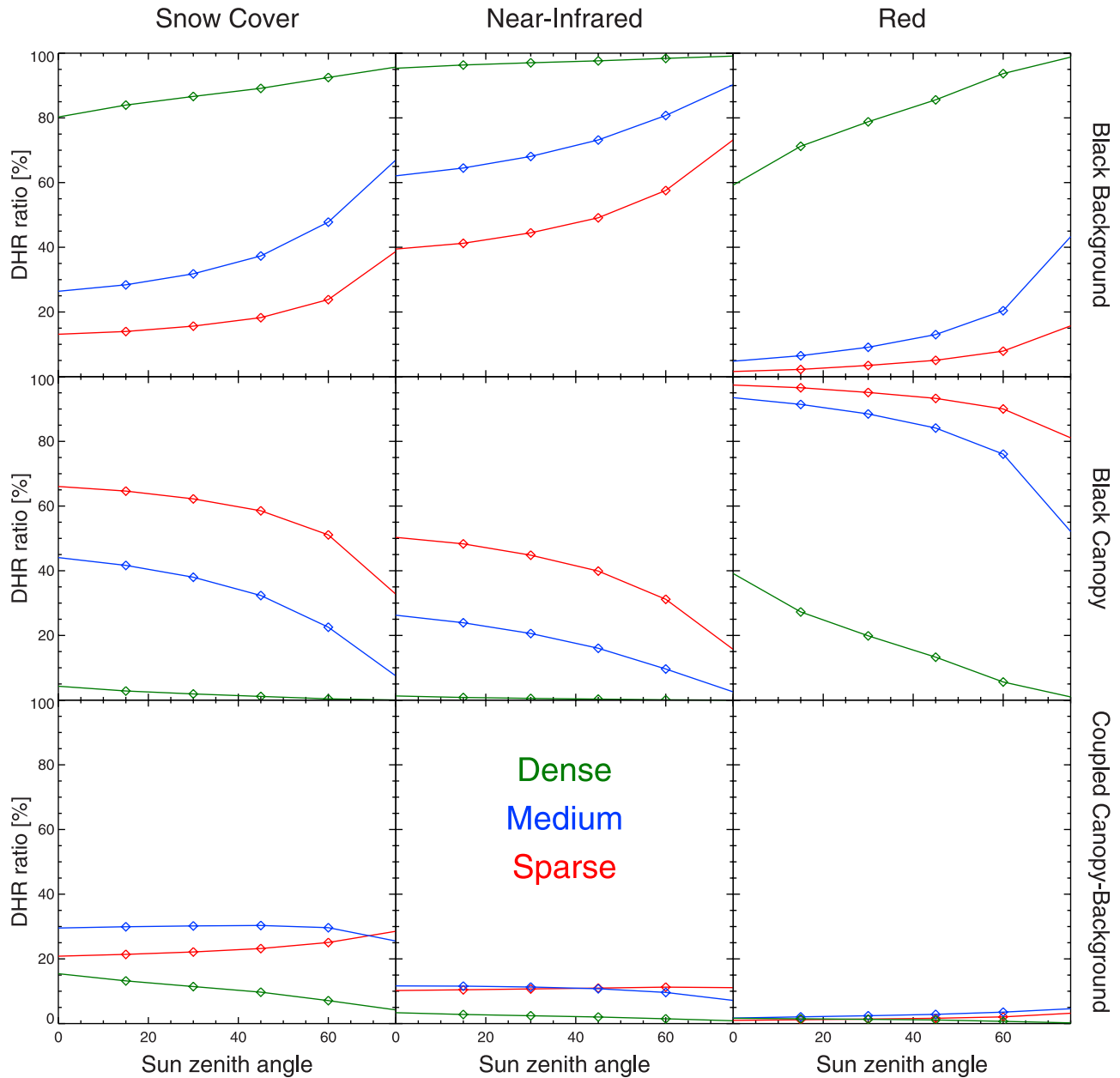
Figure 6. Relative contribution of each contributing terms in (2) to the total DHRs for the sparse, medium and dense scenarios described in Tables 1 and 2.

case of sparse, medium and dense canopy conditions. It shows that both the amplitudes and Sun angle dependencies are well reproduced by the full two-stream solutions. Indeed, the dominant contributions due to the Black Background and the Black canopy are both assessed very accurately from the procedure described here. The largest but still negligible discrepancies occurring in the near-infrared domain with a snow covered background condition are due to the term $\check{R}_{bgd}^{Coll}$ embedded into the coupled Canopy-Background contribution parameterized in section 2.6. This figure also shows that the solutions obtained in the single scattering limit provide accurate estimations in the red spectral domain but yield very significant differences in the amplitude in the near-infrared spectral domain.

[61] Figure 8 gives some numerical examples of the weighting effects induced by the diffuse radiation, on the

fraction of absorbed radiation in the visible part of the spectrum, in the case of the three 3-D scenes presented in Tables 1 and 2. These estimations use (1) to parameterize the relative direct versus diffuse contribution and are provided for two aerosol load conditions, namely for aerosol optical depth values at 0.5 μm equal to 0.1 and 0.4. The direct versus diffuse atmospheric transmission functions have been calculated as a function of the Sun zenith angle for the visible (0.3–0.7 μm) spectral range in the case of US-62 type of standard atmosphere implementing a continental aerosol model which includes a mixture of dust-like, water-soluble, and soot components [see *Vermote et al.*, 1997]. Figure 8 suggests that the contribution due to the diffuse sky illumination to the total fraction of absorbed flux, $A^{\star}(\mu_0) = A_{coupled}^{total}(\mu_0) f^{\downarrow dir}(\mu_0) + f^{\downarrow diff}(\mu_0) A_{coupled}^{total}$, can become significant, i.e., about ±0.1, when the Sun zenith
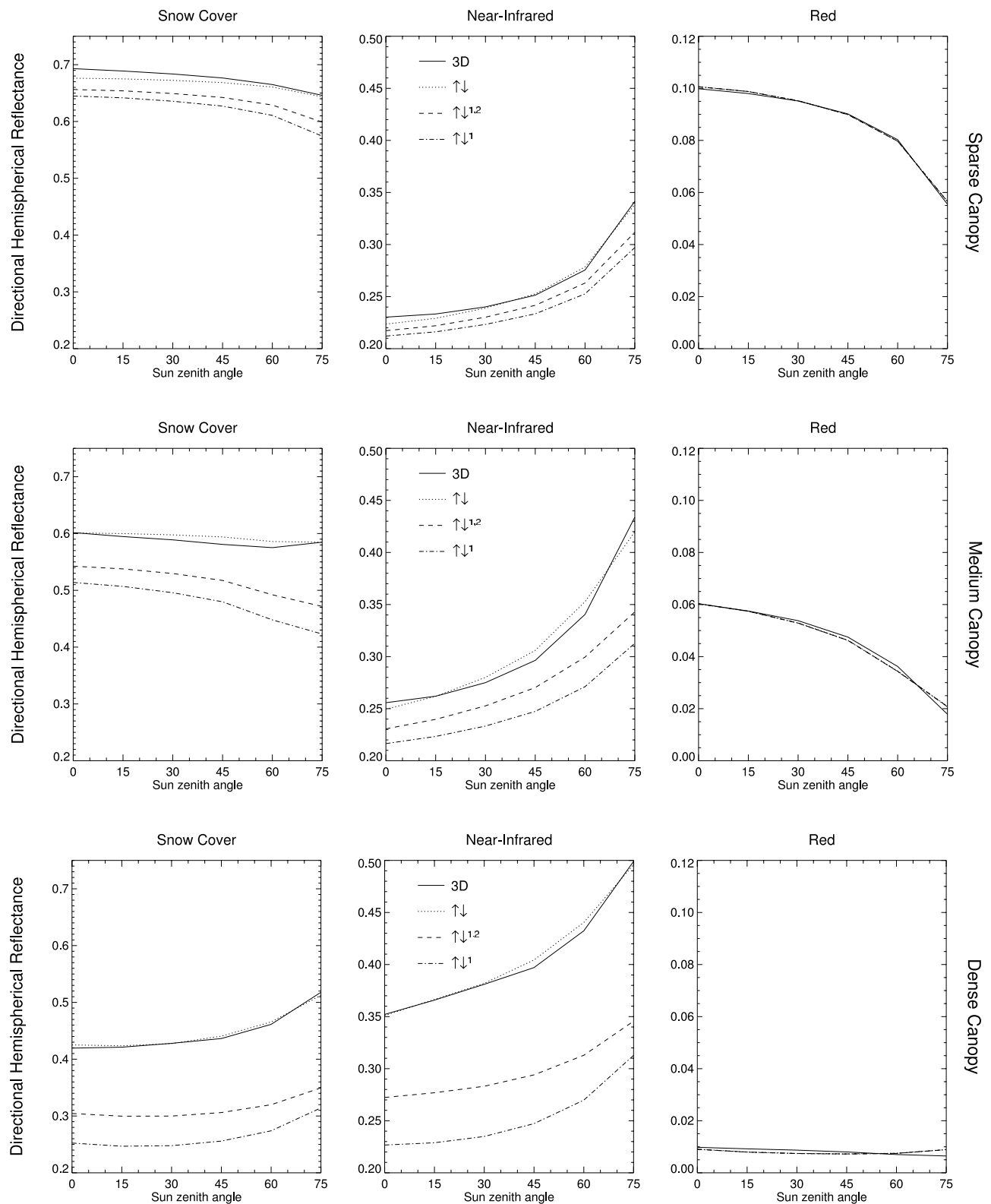
Figure 7. Comparison between the true and the two-stream based series of approximations for the DHRs in the cases of sparse, medium and dense canopy scenario. Symbols $\uparrow\downarrow$, $\uparrow\downarrow^{1s}$ and $\uparrow\downarrow^{1,2}$ identify the two-stream results obtained using the full solution, the first and the second order of scattering solutions, respectively.
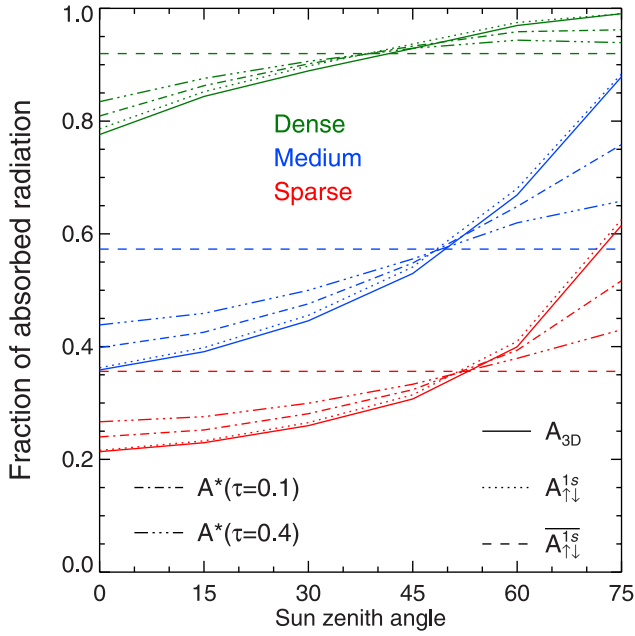
Figure 8. Fraction of absorbed flux by the vegetation with respect to direct, A_{3D} (solid line), and diffuse isotropic, $\overline{A_{\uparrow\downarrow}^{1s}}$ (dashed line), illumination only and in the visible range of the solar spectrum. Estimations obtained in the limit of single scattering, $A_{\uparrow\downarrow}^{1s}$ given by (31), are shown by the dotted lines. The dash-dotted lines correspond to the total fraction of absorbed flux, $A^{\star}(\tau)$, resulting from the direct plus the diffuse illumination together. This total flux is estimated using (1) and is given for two aerosol optical depth values at 0.5 μm equal to 0.1 and 0.4, respectively, in the case of sparse, medium and dense canopy scenarios.

angle values are either small or large. In the most frequent observation conditions at mid and high latitudes, i.e., over the range [30–60°] in Sun zenith angles, the contribution due to the diffuse radiation may be either positive or negative, but should remain somewhat limited, that is in the ±0.05 range. This figure also confirms that the single scattering approximations given by (31) and (34) provide a very good estimation of the total absorbed flux in the red spectral region of the spectrum.

[62] In order to better document the characteristics of the radiation transfer regimes associated with 3-D effects in vegetation canopies and their approximations by various modeling techniques, the three radiant fluxes corresponding to the three selected structurally heterogeneous scenes overlying a black background were compared with estimations provided by the two-stream based approximations as well as an accurate 1-D plane-parallel model. Results are summarized in Tables 6, 7, and 8, in the case of sparse, medium, and dense canopies. For each individual flux, values delivered by the 1-D 1/2 Discrete model of *Gobron et al.* [1997] and the full two-stream solution, both using the effective variable values, can be compared to the 3-D solutions.

[63] The differences between the full two-stream solutions, $F_{\uparrow\downarrow}(\widetilde{\mathbf{X}})$, and the 1-D model results, $F_{1D}(\widetilde{\mathbf{X}})$, are shown to be not significant as compared to the errors introduced by the ingestion of the true variable values, $F_{\uparrow\downarrow}(\mathbf{X})$. Indeed, not surprisingly, strong biases in all fluxes in both spectral domains are found when using the true values of the state variables. By contrast, the ingestion of the effective values of these variables yields very accurate representations of these three radiant fluxes.

[64] In the red spectral domain where absorption by vegetation is significant and, in the case of sparse and medium canopy densities, the true absorbed fluxes, i.e., accounting for the structure factor, are about twice smaller

Table 6. Reflected R_{veg}^{Coll}, Diffusely Transmitted t_{veg}^{Coll} and Absorbed A_{veg}^{Coll}, Flux Values Associated With the Black Background Contribution, With Respect to Direct Illumination Only, for a Sparse Canopy[a] $\langle LAI \rangle = 1.24$, $\langle Fc \rangle = 0.174$, in the Red and Near-Infrared Spectral Domains. The $\widetilde{r}_l$ and $\widetilde{t}_l$ Values Are Optimized Over the Range [30–60°] in Sun Zenith Angles

	$\theta_0 = 30°$	$\theta_0 = 60°$
	[b]$\widetilde{LAI} = 0.442$, $\widetilde{Fc} = 0.225$	$\widetilde{LAI} = 0.479$, $\widetilde{Fc} = 0.381$
	$T_{3D}^{dir} = T_{1D}^{dir}(\frac{\widetilde{LAI}}{2\mu_0}) = 0.7748$	$T_{3D}^{dir} = T_{1D}^{dir}(\frac{\widetilde{LAI}}{2\mu_0}) = 0.6194$
Red domain	[a]$(\langle r_l \rangle = 0.018, \langle t_l \rangle = 0.021)$ and [b]$(\widetilde{r}_l = 0.021, \widetilde{t}_l = 0.025)$	
$R_{3D}/R_{1D}(\widetilde{\mathbf{X}})/R_{\uparrow\downarrow}(\widetilde{\mathbf{X}})$[c]	3.31 10^{-3}/3.58 10^{-3}/4.05 10^{-3}	6.35 10^{-3}/6.17 10^{-3}/6.95 10^{-3}
$\mathbf{R}_{\uparrow\downarrow}(\langle\mathbf{X}\rangle)$[d]	**5.95 10^{-3}**	**8.80 10^{-3}**
$t_{3D}/t_{1D}(\widetilde{\mathbf{X}})/t_{\uparrow\downarrow}(\widetilde{\mathbf{X}})$	3.26 10^{-3}/3.98 10^{-3}/4.39 10^{-3}	7.84 10^{-3}/6.33 10^{-3}/7.09 10^{-3}
$\mathbf{t}_{\uparrow\downarrow}(\langle\mathbf{X}\rangle)/\mathbf{T}_{\uparrow\downarrow}^{dir}(\frac{\langle LAI \rangle}{2\mu_0})$	**5.64 10^{-3}/0.4887**	**7.30 10^{-3}/0.2894**
$A_{3D}/A_{1D}(\widetilde{\mathbf{X}})/A_{\uparrow\downarrow}(\widetilde{\mathbf{X}})$	0.218/0.218/0.217	0.366/0.368/0.367
$\mathbf{A}_{\uparrow\downarrow}(\langle\mathbf{X}\rangle)$	**0.4997**	**0.6945**
Near-infrared domain	[a]$(\langle r_l \rangle = 0.486, \langle t_l \rangle = 0.462)$ and [b]$(\widetilde{r}_l = 0.642, \widetilde{t}_l = 0.138)$	
$R_{3D}/R_{1D}(\widetilde{\mathbf{X}})/R_{\uparrow\downarrow}(\widetilde{\mathbf{X}})$	0.1069/0.1050/0.1102	0.1587/0.1622/0.1679
$\mathbf{R}_{\uparrow\downarrow}(\langle\mathbf{X}\rangle)$	0.2464	0.3520
$t_{3D}/t_{1D}(\widetilde{\mathbf{X}})/t_{\uparrow\downarrow}(\widetilde{\mathbf{X}})$	5.33 10^{-2}/5.34 10^{-2}/5.68 10^{-2}	0.1079/0.1079/0.1130
$\mathbf{t}_{\uparrow\downarrow}(\langle\mathbf{X}\rangle)/\mathbf{T}_{\uparrow\downarrow}^{dir}(\frac{\langle LAI \rangle}{2\mu_0})$	**0.2200/0.4887**	**0.2966/0.2894**
$A_{3D}/A_{1D}(\widetilde{\mathbf{X}})/A_{\uparrow\downarrow}(\widetilde{\mathbf{X}})$	6.48 10^{-2}/6.68 10^{-2}/5.82 10^{-2}	0.1137/0.1105/9.96 10^{-2}
$\mathbf{A}_{\uparrow\downarrow}(\langle\mathbf{X}\rangle)$	**4.50 10^{-2}**	**6.20 10^{-2}**

[a] $\langle\mathbf{X}\rangle$ identifies the true value of variable $\mathbf{X}$, i.e., in the 3-D representation.
[b] $\widetilde{\mathbf{X}}$ identifies the effective value of variable $\mathbf{X}$ (see *Pinty et al.* [2004] and section 2.3).
[c] $F_{3D}/F_{1D}(\widetilde{\mathbf{X}})/F_{\uparrow\downarrow}(\widetilde{\mathbf{X}})$: Flux $\mathbf{F}$ value estimated with 3-D/1-D/two-stream models.
[d] $F_{\uparrow\downarrow}(\langle\mathbf{X}\rangle)$: Flux $\mathbf{F}$ value estimated with a two-stream model using true variable values.

Table 7. Reflected R_{veg}^{Coll}, Diffusely Transmitted t_{veg}^{Coll} and Absorbed A_{veg}^{Coll}, Flux Values Associated With the Black Background Contribution, With Respect to Direct Illumination Only, for a Medium Canopy[a] $\langle LAI\rangle$ = 2.0, $\langle Fc\rangle$ = 0.303, in the Red and Near-Infrared Spectral Domains. The $\widetilde{r_l}$ and $\widetilde{t_l}$ Values Are Optimized Over the Range [30–60°] in Sun Zenith Angles

	$\theta_0 = 30°$	$\theta_0 = 60°$
	[b]$\widetilde{LAI}$ = 0.896, $\widetilde{Fc}$ = 0.404 $T_{3D}^{dir} = T_{1D}^{dir}(\frac{\langle LAI\rangle}{2\mu_0})$ = 0.5961	$\widetilde{LAI}$ = 1.061, $\widetilde{Fc}$ = 0.638 $T_{3D}^{dir} = T_{1D}^{dir}(\frac{\langle LAI\rangle}{2\mu_0})$ = 0.3462
Red domain	[a]$(\langle r_l\rangle$ = 0.018, $\langle t_l\rangle$ = 0.021) and [b]$(\widetilde{r_l}$ = 0.017, $\widetilde{t_l}$ = 0.027)	
$R_{3D}/R_{1D}(\widetilde{X})/R_{\uparrow\downarrow}(\widetilde{X})$[c]	4.91 10⁻³/5.43 10⁻³/5.38 10⁻³	7.38 10⁻³/8.74 10⁻³/9.10 10⁻³
$\mathbf{R_{\uparrow\downarrow}(\langle X\rangle)}$[d]	**6.67 10⁻³**	**9.50 10⁻³**
$t_{3D}/t_{1D}(\widetilde{X})/t_{\uparrow\downarrow}(\widetilde{X})$	5.15 10⁻³/5.72 10⁻³/6.48 10⁻³	9.50 10⁻³/7.78 10⁻³/8.85 10⁻³
$\mathbf{t_{\uparrow\downarrow}(\langle X\rangle)\ T_{\uparrow\downarrow}^{dir}(\frac{\langle LAI\rangle}{2\mu_0})}$	**5.13 10⁻³/0.3151**	**5.60 10⁻³/0.1353**
$A_{3D}(\langle X\rangle)/A_{1D}(\widetilde{X})/A_{\uparrow\downarrow}(\widetilde{X})$	0.393/0.393/0.392	0.637/0.637/0.636
$\mathbf{A_{\uparrow\downarrow}(\langle X\rangle)}$	**0.673**	**0.850**
Near-infrared domain	[a]$(\langle r_l\rangle$ = 0.486, $\langle t_l\rangle$ = 0.462) and [b]$(\widetilde{r_l}$ = 0.680, $\widetilde{t_l}$ = 0.118)	
$R_{3D}/R_{1D}(\widetilde{X})/R_{\uparrow\downarrow}(\widetilde{X})$	0.1873/0.1870/0.1932	0.2748/0.2770/0.2863
$\mathbf{R_{\uparrow\downarrow}(\langle X\rangle)}$	**0.3364**	**0.4490**
$t_{3D}/t_{1D}(\widetilde{X})/t_{\uparrow\downarrow}(\widetilde{X})$	9.08 10⁻²/9.20 10⁻²/9.90 10⁻²	0.1685/0.1651/0.1778
$\mathbf{t_{\uparrow\downarrow}(\langle X\rangle)\ T_{\uparrow\downarrow}^{dir}(\frac{\langle LAI\rangle}{2\mu_0})}$	**0.2710/0.3151**	**0.3184/0.1353**
$A_{3D}/A_{1D}(\widetilde{X})/A_{\uparrow\downarrow}(\widetilde{X})$	0.1240/0.1249/0.1117	0.210/0.2117/0.1897
$\mathbf{A_{\uparrow\downarrow}(\langle X\rangle)}$	**7.70 10⁻²**	**9.70 10⁻²**

[a]$\langle X\rangle$ identifies the true value of variable **X**, i.e., in the 3-D representation.
[b]$\widetilde{X}$ identifies the effective value of variable **X** (see *Pinty et al.* [2004] and section 2.3).
[c]$F_{3D}/F_{1D}(\widetilde{X})/F_{\uparrow\downarrow}(\widetilde{X})$: Flux **F** value estimated with 3-D/1-D/two-stream models.
[d]$F_{\uparrow\downarrow}(\langle X\rangle)$: Flux **F** value estimated with a two-stream model using true variable values.

that those obtained when using the true LAI of the scene. This result has very significant implications when estimating, from allometric LAI values, the fraction of absorbed radiation in the spectral domain useful for vegetation photosynthesis process. One can also notice that the absorbed fraction by the Black Background component, $A_{\uparrow\downarrow}(\widetilde{X})$, is, as expected from (31), indeed very close to the radiation intercepted by the background, $\widetilde{Fc}$.

[65] In the near-infrared domain, the use of the effective, as opposed to the true, state variable values translates into a very different distribution of the incoming flux into the reflected and transmitted components. For example, albedo values appear to be overestimated by a factor of about two when neglecting the structure factor effects. These results have thus significant implications for further studies aiming at modeling these fluxes on the basis of input values such as

Table 8. Reflected R_{veg}^{Coll}, Diffusely Transmitted t_{veg}^{Coll} and Absorbed A_{veg}^{Coll}, Flux Values Associated With the Black Background Contribution, With Respect to Direct Illumination Only, for a Dense Canopy[a] $\langle LAI\rangle$ = 4.82, $\langle Fc\rangle$ = 0.869, in the Red and Near-Infrared Spectral Domains. The $\widetilde{r_l}$ and $\widetilde{t_l}$ Values Are Optimized Over the Range [30–60°] in Sun Zenith Angles

	$\theta_0 = 30°$	$\theta_0 = 60°$
	[b]$\widetilde{LAI}$ = 3.677, $\widetilde{Fc}$ = 0.928 $T_{3D}^{dir} = T_{1D}^{dir}(\frac{\langle LAI\rangle}{2\mu_0})$ = 0.1197	$\widetilde{LAI}$ = 3.667, $\widetilde{Fc}$ = 0.975 $T_{3D}^{dir} = T_{1D}^{dir}(\frac{\langle LAI\rangle}{2\mu_0})$ = 2.55 10⁻²
Red domain	[a]$(\langle r_l\rangle$ = 0.018, $\langle t_l\rangle$ = 0.021) and [b]$(\widetilde{r_l}$ = 0.015, $\widetilde{t_l}$ = 0.023)	
$R_{3D}/R_{1D}(\widetilde{X})/R_{\uparrow\downarrow}(\widetilde{X})$[c]	6.81 10⁻³/7.51 10⁻³/6.24 10⁻³	6.55 10⁻³/1.01 10⁻²/9.01 10⁻³
$\mathbf{R_{\uparrow\downarrow}(\langle X\rangle)}$[d]	**7.00 10⁻³**	**9.70 10⁻³**
$t_{3D}/t_{1D}(\widetilde{X})/t_{\uparrow\downarrow}(\widetilde{X})$	3.00 10⁻³/3.59 10⁻³/2.84 10⁻³	2.40 10⁻³/2.63 10⁻³/1.99 10⁻³
$\mathbf{t_{\uparrow\downarrow}(\langle X\rangle)\ T_{\uparrow\downarrow}^{dir}(\frac{\langle LAI\rangle}{2\mu_0})}$	**1.70 10⁻³/6.18 10⁻²**	**8.20 10⁻⁴/8.01 10⁻³**
$A_{3D}(\langle X\rangle)/A_{1D}(\widetilde{X})/A_{\uparrow\downarrow}(\widetilde{X})$	0.871/0.869/0.871	0.965/0.962/0.963
$\mathbf{A_{\uparrow\downarrow}(\langle X\rangle)}$	**0.930**	**0.981**
Near-infrared domain	[a]$(\langle r_l\rangle$ = 0.486, $\langle t_l\rangle$ = 0.462) and [b]$(\widetilde{r_l}$ = 0.728, $\widetilde{t_l}$ = 0.102)	
$R_{3D}/R_{1D}(\widetilde{X})/R_{\uparrow\downarrow}(\widetilde{X})$	0.3668/0.3664/0.3733	0.4231/0.4270/0.4414
$\mathbf{R_{\uparrow\downarrow}(\langle X\rangle)}$	**0.4932**	**0.5861**
$t_{3D}/t_{1D}(\widetilde{X})/t_{\uparrow\downarrow}(\widetilde{X})$	0.1236/0.1248/0.1306	0.1308/0.1227/0.1261
$\mathbf{t_{\uparrow\downarrow}(\langle X\rangle)\ T_{\uparrow\downarrow}^{dir}(\frac{\langle LAI\rangle}{2\mu_0})}$	**0.2413/6.18 10⁻²**	**0.2012/8.01 10⁻³**
$A_{3D}/A_{1D}(\widetilde{X})/A_{\uparrow\downarrow}(\widetilde{X})$	0.3768/0.3860/0.3765	0.4181/0.4248/0.4069
$\mathbf{A_{\uparrow\downarrow}(\langle X\rangle)}$	**0.2037**	**0.2046**

[a]$\langle X\rangle$ identifies the true value of variable **X**, i.e., in the 3-D representation.
[b]$\widetilde{X}$ identifies the effective value of variable **X** (see *Pinty et al.* [2004] and section 2.3).
[c]$F_{3D}/F_{1D}(\widetilde{X})/F_{\uparrow\downarrow}(\widetilde{X})$: Flux **F** value estimated with 3-D/1-D/two-stream models.
[d]$F_{\uparrow\downarrow}(\langle X\rangle)$: Flux **F** value estimated with a two-stream model using true variable values.

LAI which, if correct, are as close as possible to their true values.

4. Conclusions

[66] The 1-D approaches, such as the two-stream schemes implemented in GCMs to represent land surface processes in general, and more specifically the radiation transfer regimes occurring in 3-D structurally heterogeneous environments, impose the use of effective variables in order to (1) accurately model the three radiant fluxes for realistic conditions, (2) validate the GCM outputs against the values delivered by remote sensing algorithms, and (3) ensure the consistency between various fluxes and state variable values when using assimilation techniques. The definition of effective variables follows from simple radiation transfer considerations, such as satisfying the classical Beer-Bouger-Lambert law for the extinction of the direct illumination while, in the mean time, ensuring a correct distribution between the reflected, diffusely transmitted and absorbed fluxes associated with 3-D structurally heterogeneous conditions. The inverse procedure to estimate the values of the effective variables is fully described in *Pinty et al.* [2004].

[67] It was shown that adopting effective variable values necessitates the introduction of an additional parameter in the classical 1-D radiation transfer problem, namely a structure factor, embedding the radiative effects due to the spatial variability of the leaf density. This has motivated a revisit and adaptation of the existing two-stream formulations and their associated solutions in order to cope with this new requirement. Our two-stream solutions, as well as their approximations, for estimating the three radiant fluxes accurately are decomposed into separate contributions, namely the Black Background (no scattering from the background), the Black Canopy (no scattering by canopy elements) and the remaining contribution involving multiple scattering events between the canopy and the background. This decomposition facilitates the identification of the physical processes intervening in the various components. The Black Background solutions follow exactly the *Meador and Weaver*'s [1980] original two-stream solutions for direct illumination conditions. It was shown from various simulation exercises that the latter deliver very accurate results provided they are used with the effective instead of the true state variable values, that is they account for the structure factor. The solution to the Black Canopy problem is accurately represented via an approximate function involving the value of the structure factor estimated at 60° Sun zenith angle. Finally the coupled canopy-background scattering processes are parameterized on the basis of the same *Meador and Weaver*'s [1980] two-stream solutions but extended to address the case of an external isotropic source of illumination.

[68] The two-stream solutions were found to be in very good agreement with results from accurate and realistic simulations of 3-D heterogeneous canopies, as represented by a Monte-Carlo model, both for standard and extreme conditions, in both the red and near-infrared spectral regions. Two-stream approaches can thus be used with confidence, provided the updated formulae and the structure factor are implemented. The expected biome to biome variability of the structure factor and the associated effective variables can be estimated using 3-D Monte-Carlo simulations of realistic canopy conditions. The former can also be assessed in the field using appropriate instruments such as the Tracking Radiation and Architecture of Canopies (TRAC) [*Chen and Cihlar*, 1995].

[69] Under typical vegetation conditions, this structure factor takes on values much smaller than unity when the canopy structure deviates from the plane-parallel structurally homogeneous case. Since this factor weights the domain-averaged true LAI value (in addition to the 1/2 coefficient when considering a spherical leaf angle distribution function), it exerts a strong control (about a factor of 2) on the fraction of absorbed (in the spectral regions where leaf absorption is important) and reflected fluxes (in the spectral regions where scattering processes dominates). In other words, the ingestion of true LAI and leaf reflectance and transmitance values into a standard 1-D radiation transfer scheme, can only yield significantly erroneous estimations of the reflected, transmitted and absorbed fluxes. Since it is not possible to estimate jointly the correct values of these three fluxes without weighting the true values of the state variables, such as LAI, by the structure factor, it implies that the remote sensing products, when retrieved from 3-D radiation transfer models should not be ingested as such by 1-D plane-parallel modeling schemes.

[70] The introduction of an additional parameter, representing the effects due to the internal variability of the canopy density, to generate the correct radiation transfer regimes into 3-D canopies is proposed such that it ensures the transition from the homogeneous turbid to the structurally heterogeneous cases. Indeed the structure factor varies smoothly from exactly unity in the homogeneous turbid case to smaller values as the vegetation heterogeneity becomes more significant. This should prove useful for investigating further land surface processes controlling not only the radiation but also the heat, water and CO_2 fluxes.

Appendix A: Two-Stream Solutions for Homogeneous Canopies With Preferred Leaf Orientations

[71] The two-stream or two-flux problem can be set in multiple mathematical ways, depending, for instance, on the associated treatment of the external top and bottom boundary conditions, that is the direct and diffuse types of illumination impinging on the top and arising from the bottom of the vegetation layer. Since we have opted for the unified system of equations laid out by *Meador and Weaver* [1980], the remaing issue to be solved here concerns the derivation of the relevant expressions for the $\omega \beta$ and $\omega \beta_0$ (μ_0) parameters that represent the backscattered fraction over the hemisphere with respect to diffuse and direct radiation, respectively.

[72] In the specific case of structurally homogeneous turbid vegetation canopy layers, the elementary scatterers are modeled as oriented plates of infinitely small size. Depending on the vegetation type and environmental conditions, the orientation probability of the normals to these plates, namely $f(\theta_l, \phi_l)$, may follow various distributions including planophile, erectophile, and even heliotropic. Once the leaf angle probability distribution function is

Table A1. Expressions for the γ Coefficients Required in the Two-Stream Formulation Proposed by *Meador and Weaver* [1980, equations (14) and (15)] in the Case of Vegetation Composed of Leaves Exhibiting Spherical, Planophile, and Erectophile Orientation Probability Distributions[a] With $\omega_l = (\widetilde{r_l} + \widetilde{t_l})$ and $\delta_l = (\widetilde{r_l} - \widetilde{t_l})$

γ_1	γ_2	γ_3	γ_4
[b]$[\bar{\mu}\, G(\mu_0)]^{-1}\, [1 - \frac{\omega_l}{2} + \frac{\delta_l}{\eta}]$[c]	[b]$[\bar{\mu} G(\mu_0)]^{-1}\, [\frac{\omega_l}{2} + \frac{\delta_l}{\eta}]$[c]	$[\frac{\omega_l}{2} + \frac{\mu_0}{G(\mu_0)\eta}\frac{\delta_l}{}]$[c]$/\omega_l$	$1 - \gamma_3$

[a]Taken from *Bunnik* [1978].

[b]$\bar{\mu}$ values ($\bar{\mu} = \int_0^1 \mu' \times G(\mu')^{-1} d\mu'$ [after *Dickinson*, 1983]), are close to 0.9065 and 1.046 for planophile and erectophile orientation probability distributions, respectively, and equal to 1 for the spherical case.

[c]The η coefficient is equal to 6, 8/3 and 8 for spherical, planophile, and erectophile orientation probability distributions, respectively.

given, it becomes feasible to express the extinction coefficient of any elementary volume and thus the total extinction of the vertically homogeneous vegetation layer [e.g., *Ross*, 1981; *Dickinson*, 1983; *Verstraete*, 1987]. This extinction coefficient, traditionally expressed with *Ross*'s [1981] G function, thus modulates the optical thickness of the homogeneous vegetation layer. In the simplest case of a spherical orientation probability distribution in θ_l assuming a uniform probability distribution in ϕ_l, i.e., $f(\theta_l) = 1$, the G function is constant and equal to 1/2.

[73] The $\omega\,\beta$ and $\omega\,\beta_0\,(\mu_0)$ parameters that ultimately enter the *Meador and Weaver*'s [1980] γ coefficients should thus be expressed via the G function and the leaf orientation probability distribution. The $\omega\,\beta$ parameter has been derived by *Norman and Jarvis* [1975] in the case of a single leaf whose normal is oriented at zenith angle θ_l from the local vertical defined in the upward hemisphere:

$$\omega\beta = \frac{1}{2}\left(\omega_l + \delta_l \cos^2(\theta_l)\right) \quad (A1)$$

[74] Since (A1) is valid for one single leaf only, its integral over the appropriate leaf orientation probability distribution has to be performed between 0 and $\pi/2$ because the leaf normals are assumed to be oriented into the upward hemisphere, that is:

$$\omega\beta = \frac{1}{2}\left(\omega_l + \delta_l \int_0^{\pi/2} \cos^2\theta_l\, f(\theta_l)\, \sin\theta_l\, d\theta_l\right) \quad (A2)$$

and,

$$\omega\beta_0(\mu_0) = \frac{1}{2}\left(\omega_l + \frac{\mu_0}{G(\mu_0)}\delta_l \int_0^{\pi/2} \cos^2\theta_l\, f(\theta_l)\, \sin\theta_l\, d\theta_l\right) \quad (A3)$$

where $\sin\theta_l$ is introduced for normalization requirement of the probability distribution function. Various distributions are available from the literature [e.g., *Bunnik*, 1978; *Goel and Strebel*, 1984; *Nilson and Kuusk*, 1989] and any of those can be chosen to derive an analytical solution to the backscatter parameters. For example, the trigonometric functions, equivalent to $f(\theta_l)\sin\theta_l$, proposed by Bunnik in the case of spherical, planophile and erectophile distributions yield formulations for the *Meador and Weaver*'s [1980] γ coefficients that are summarized in Table A1. The resulting two-stream solutions with regard to the albedo, R_{veg}^{Coll}, and the diffuse transmission factors, T_{veg}^{Coll} deliver quite accurate results for the leaf orientation probability distributions we considered here.

[75] The diversity of notations used by the authors of two-stream formulations and, in some instances, the derivation of explicit formula for the scattered flux only, make it uneasy to ensure that our proposed set of γ coefficients are equivalent to those published previously [e.g., *Verhoef*, 1984; *Nilson*, 1991; *Kuusk*, 2001]. They are, however, different from those adopted in the radiation transfer scheme of the SImple Biosphere model [*Sellers et al.*, 1996] at least in the case of leaf anisotropic scattering conditions. The latter model is in fact strictly valid and accurate only in the case of structurally homogeneous canopies composed of leaves satisfying a spherical leaf angle probability distribution and a fully isotropic scattering function, that is $\widetilde{r_l} = \widetilde{t_l}$. Any departure from this condition may yield seriously erroneous estimations of the radiant fluxes because of a simplified/approximate formulation of the results from (A2) and (A3). The two-stream solutions proposed in Tables A1 and 4 also enclose an explicit and more accurate formulation of the backscatter parameter, $\omega\,\beta_0$, with respect to the direct source which simplifies the approach originally suggested by *Dickinson* [1983].

Appendix B: Two-Stream Solutions for All Orders of Scattering

[76] Following *Meador and Weaver*'s [1980, equations (12) and (13)] approach and adapting their notations to the vegetation problem that is $\tau' = \widetilde{LAI'}\, G(\mu_0)$, the set of equations leading to two-stream generic solutions, in the case of a plane-parallel vegetation layer illuminated by a collimated flux of radiation $\pi\,F$, is expressed as follows:

$$\frac{dI^+}{G(\mu_0)\, d\widetilde{LAI'}} = \gamma_1 I^+ - \gamma_2 I^- - \pi F\, \gamma_3\, \omega_l \exp\left(-G(\mu_0)\,\widetilde{LAI'}/\mu_0\right)$$

$$\frac{dI^-}{G(\mu_0)\, d\widetilde{LAI'}} = \gamma_2 I^+ - \gamma_1 I^- + \pi F\, \gamma_4\, \omega_l \exp\left(-G(\mu_0)\,\widetilde{LAI'}/\mu_0\right)$$

(B1)

where I^+ and I^- represent the upward and downward hemispherical radiation flux associated to an external collimated source of radiation, respectively. $G(\mu_0)$ is the so-called Ross's function expressing the leaf extinction coefficient in elementary layers of a turbid vegetation layer whose total effective optical thickness is $\widetilde{LAI}$. Solving (B1) for boundary conditions $I^- = 0$ at the top (radiation source is a beam collimated around direction μ_0 only) and $I^+ = 0$ at the bottom (the black background condition) yields expressions for the Directional Hemispherical Reflectance and total transmission factor, respectively:

$$R_{veg}^{Coll}(z_{toc},\mu_0) = \frac{\omega_l}{(1 - k^2\mu_0^2)\left[(k+\gamma_1)\exp\left(k\,G(\mu_0)\,\widetilde{LAI}\right) + (k-\gamma_1)\exp\left(-k\,G(\mu_0)\,\widetilde{LAI}\right)\right]}$$
$$\cdot \left[(1-k\mu_0)(\alpha_2 + k\gamma_3)\exp\left(k\,G(\mu_0)\,\widetilde{LAI}\right)\right.$$
$$- (1+k\mu_0)(\alpha_2 - k\gamma_3)\exp\left(-k\,G(\mu_0)\,\widetilde{LAI}\right)$$
$$\left. - 2\,k\,(\gamma_3 - \alpha_2\mu_0)\exp\left(-G(\mu_0)\,\widetilde{LAI}/\mu_0\right)\right] \tag{B2}$$

and,

$$T_{veg}^{Coll}(z_{bgd},\mu_0) = \exp\left(-G(\mu_0)\,\widetilde{LAI}/\mu_0\right)$$
$$\left\{1 - \frac{\omega_l}{(1-k^2\mu_0^2)\left[(k+\gamma_1)\exp\left(k\,G(\mu_0)\,\widetilde{LAI}\right) + (k-\gamma_1)\exp\left(-k\,G(\mu_0)\,\widetilde{LAI}\right)\right]}\right.$$
$$\cdot \left[(1+k\mu_0)(\alpha_1 + k\gamma_4)\exp\left(k\,G(\mu_0)\,\widetilde{LAI}\right)\right.$$
$$- (1-k\mu_0)(\alpha_1 - k\gamma_4)\exp\left(-k\,G(\mu_0)\,\widetilde{LAI}\right)$$
$$\left.\left. - 2\,k\,(\gamma_4 + \alpha_1\mu_0)\exp\left(G(\mu_0)\,\widetilde{LAI}/\mu_0\right)\right]\right\} \tag{B3}$$

with

$$\alpha_1 = \gamma_1\gamma_4 + \gamma_2\gamma_3$$
$$\alpha_2 = \gamma_1\gamma_3 + \gamma_2\gamma_4$$
$$k = \left(\gamma_1^2 - \gamma_2^2\right)^{1/2}$$
$$1 = \gamma_3 + \gamma_4 \tag{B4}$$

where the appropriate values of the γ coefficients are given in Tables A1 and 4. Note that in the particular case of a spherical leaf angle distribution function, we have $G(\mu_0) = 0.5$.

[77] A second set of two-stream equations, analogous to (B1), can be established straightforwardly by replacing the transmission of the external collimated source, $\exp(-G(\mu_0) LAI'/\mu_0)$, by the one corresponding to the external isotropic source, thus equivalent to $\overline{T_{veg}^{UnColl}}$ (see (14)). For the usual range of canopy optical depth values, $\overline{R_{veg}^{Coll}}(z_{toc})$ and $\overline{T_{veg}^{Coll}}(z_{bgd})$ can be estimated with (B2) and (B3) again, and replacing simply μ_0 by $\mu_0 = 0.5/0.705$ (in (B2), (B3), and the γ_i's coefficients). The empirical weighting factor equals to 0.705 has been introduced in section 2.5 as a simple way to provide a numerically accurate solution to $\overline{T_{veg}^{UnColl}}$. (B2) and (B3) are therefore the only equations needed to estimate both the directional hemispherical and bi-hemispherical fluxes.

References

Abramowitz, M., and I. A. Stegun (1970), *Handbook of Mathematical Functions*, 1045 pp., Dover, Mineola, N. Y.

Avissar, R., and M. M. Verstraete (1990), The representation of continental surface processes in mesoscale atmospheric models, *Rev. Geophys.*, *28*, 35–52.

Boissé, P. (1990), Radiative transfer inside clumpy media: The penetration of UV photons inside clumpy clouds, *Astron. Astrophys.*, *228*, 483–501.

Bunnik, N. J. J. (1978), The multispectral reflectance of shortwave radiation of agricultural crops in relation with their morphological and optical properties, technical report, Mededelingen Landbouwhogeschool, Wageningen, Netherlands.

Burke, E. J., W. J. Shuttleworth, Z.-L. Yang, S. L. Mullen, and M. A. Arain (2000), The impact of parameterization of heterogeneous vegetation on the modeled large-scale circulation in CCM3-BATS, *Geophys. Res. Lett.*, *27*, 397–400.

Cahalan, R. F., W. Ridgway, W. J. Wiscombe, T. L. Bell, and J. B. Snider (1994), The albedo of fractal stratocumulus clouds, *J. Atmos. Sci.*, *51*, 2434–2455.

Cairns, B., A. Lacis, and B. Carlson (2000), Absorption within inhomogeneous clouds and its parameterization in general circulation models, *J. Atmos. Sci.*, *57*, 700–714.

Chen, J. M., and J. Cihlar (1995), Plant canopy gap size analysis theory for improving optical measurements of leaf area index, *Appl. Opt.*, *34*, 6211–6222.

Chen, J. M., P. D. Blanken, T. A. Black, M. Guilbeault, and S. Chen (1997a), Radiation regime and canopy architecture in a boreal Aspen forest, *Agric. For. Meteorol.*, *86*, 107–125.

Chen, J. M., P. M. Rich, S. T. Gower, J. M. Norman, and S. Plummer (1997b), Leaf area index of boreal forests: Theory, techniques, and measurements, *J. Geophys. Res.*, *102*(D24), 29,429–29,443.

Coakley, J. A., and P. Chylek (1975), The two-stream approximation in radiative transfer: Including the angle of incident radiation, *J. Atmos. Sci.*, *32*, 409–418.

Dai, Y., et al. (2003), The common land model, *Bull. Am. Meteorol. Soc.*, *84*, 1013–1023.

Davis, A. B., and A. Marshak (2004), Photon propagation in heterogeneous optical media with spatial correlations: Enhanced mean free-paths and wider-than-exponential free-path distributions, *J. Quant. Spectrosc. Radiat. Transfer*, *84*, 3–34.

Dickinson, R. E. (1983), Land surface processes and climate—Surface albedos and energy balance, *Adv. Geophys.*, *25*, 305–353.

Dickinson, R. E., A. Henderson-Sellers, P. J. Kennedy, and M. F. Wilson (1986), Biosphere Atmosphere Transfer Scheme (BATS) for the NCAR Community Climate Model, *Tech. Note TN275+STR*, Natl. Cent. for Atmos. Res.

Diner, D. J., et al. (2005), The value of multiangle measurements for retrieving structurally and radiatively consistent properties of clouds, aerosols and surfaces, *Remote Sens. Environ.*, in press.

Dozier, J. (1989), Spectral signature of alpine snow cover from the Landsat Thematic Mapper, *Remote Sens. Environ.*, *28*, 9–22.

Gerard, F. F., and P. R. J. North (1997), Analyzing the effect of structural variability and canopy gaps on forest BRDF using a geometric-optical model, *Remote Sens. Environ.*, *62*, 46–62.

Gobron, N., B. Pinty, M. M. Verstraete, and Y. Govaerts (1997), A semi-discrete model for the scattering of light by vegetation, *J. Geophys. Res.*, *102*, 9431–9446.

Gobron, N., B. Pinty, M. M. Verstraete, and Y. Govaerts (1999), The MERIS Global Vegetation Index (MGVI): Description and preliminary application, *Int. J. Remote Sens.*, *20*, 1917–1927.

Goel, N. S., and D. E. Strebel (1984), Simple beta distribution representation of leaf orientation in vegetation canopies, *Agron. J.*, *76*, 800–803.

Govaerts, Y., and M. M. Verstraete (1998), Raytran: A Monte Carlo ray tracing model to compute light scattering in three-dimensional heterogeneous media, *IEEE Trans. Geosci. Remote Sens.*, *36*, 493–505.

Jensen, J. (1906), Sur les fonctions convexes et les inégalités entre les valeurs moyennes, *Acta Math.*, *30*, 789–806.

Knyazikhin, Y., J. Kranigk, R. B. Myneni, O. Panfyorov, and G. Gravenhorst (1998a), Influence of small-scale structure on radiative transfer and photosynthesis in vegetation canopies, *J. Geophys. Res.*, *103*, 6133–6144.

Knyazikhin, Y., J. V. Martonchik, D. J. Diner, R. B. Myneni, M. M. Verstraete, B. Pinty, and N. Gobron (1998b), Estimation of vegetation canopy leaf area index and fraction of absorbed photosynthetically active radiation from atmosphere-corrected MISR data, *J. Geophys. Res.*, *103*, 32,239–32,256.

Kondratyev, K. (1972), *Radiation Processes in the Atmosphere*, 214 pp., World Meteorol. Org., Geneva, Switzerland.

Kostinski, A. B. (2001), On the extinction of radiation by a homogeneous but spatially correlated random medium, *J. Opt. Soc. Am. A*, *18*, 1929–1933.

Kuusk, A. (2001), A two-layer canopy reflectance model, *J. Quant. Spectrosc. Radiat. Transfer*, *71*, 1–9.

Lewis, P., and M. Barnsley (1994), Influence of the sky radiance distribution on various formulations of the Earth surface albedo, in *Proceedings of the 6th ISPRS International Symposium on Physical Measurements and Signatures in Remote Sensing, Val d'Isère, France, 17–21 January 1994*, pp. 707–715, CNES.

Li, X., A. H. Strahler, and C. E. Woodcock (1995), A hybrid geometric optical radiative transfer approach for modeling albedo and directional reflectance of discontinuous canopies, *IEEE Trans. Geosci. Remote Sens.*, *33*, 466–480.

Martonchik, J. V., D. J. Diner, B. Pinty, M. M. Verstraete, R. B. Myneni, Y. Knyazikhin, and H. R. Gordon (1998), Determination of land and ocean reflective, radiative, and biophysical properties using multiangle imaging, *IEEE Trans. Geosci. Remote Sens.*, *36*, 1266–1281.

Martonchik, J. V., C. J. Bruegge, and A. H. Strahler (2000), A review of reflectance nomenclature for remote sensing, *Remote Sens. Rev. IWMMM-2 Special Issue*, 9–20.

Meador, W. E., and W. R. Weaver (1980), Two-stream approximations to radiative transfer in planetary atmospheres: A unified description of existing methods and new improvements, *J. Atmos. Sci.*, *37*, 630–643.

Myneni, R. B., et al. (2002), Global products of vegetation leaf area and fraction absorbed PAR from year one of MODIS data, *Remote Sens. Environ.*, *83*, 214–231.

Nicodemus, F. E., J. C. Richmond, J. J. Hsia, I. W. Ginsberg, and T. Limperis (1977), Geometrical considerations and nomenclature for reflectance, *NBS Monogr. 160*, Natl. Bur. of Stand., U.S. Dep. of Commer., Washington, D. C.

Nilson, T. (1971), A theoretical analysis of the frequency of gaps in plant stands, *Agric. Meteorol.*, *8*, 25–38.

Nilson, T. (1991), Approximate analytical methods for calculating the reflection functions of leaf canopies in remote sensing applications, in *Photon-Vegetation Interactions*, edited by R. B. Myneni and J. Ross, pp. 163–189, Springer, New York.

Nilson, T., and A. Kuusk (1989), A reflectance model for the homogeneous plant canopy and its inversion, *Remote Sens. Environ.*, *27*, 157–167.

Niu, G.-Y., and Z.-L. Yang (2004), Effects of vegetation canopy processes on snow surface energy and mass balance, *J. Geophys. Res.*, *109*, D23111, doi:10.1029/2004JD004884.

Norman, J. M., and P. G. Jarvis (1975), Photosynthesis in Sitka Spruce (Picea Sitchensis) and a test case, *J. Appl. Ecol.*, *12*, 839–878.

Oker-Blom, P., J. Lappi, and H. Smolander (1991), Radiation regime and photosynthesis of coniferous stands, in *Photon-Vegetation Interactions*, edited by R. B. Myneni and J. Ross, pp. 471–496, Springer, New York.

Painter, T. H., and J. Dozier (2004), Measurements of the hemispherical-directional reflectance of snow at fine spectral and angular resolution, *J. Geophys. Res.*, *109*, D18115, doi:10.1029/2003JD004458.

Panferov, O., Y. Knyazikhin, R. B. Myneni, J. Szarzynski, E. Engwald, K. G. Schnitzler, and G. Gravenhorst (2001), The role of canopy structure in the spectral variation of transmission and absorption of solar radiation in vegetation canopies, *IEEE Trans. Geosci. Remote Sens.*, *39*, 241–253.

Pinty, B., N. Gobron, J.-L. Widlowski, T. Lavergne, and M. M. Verstraete (2004), Synergy between 1-D and 3-D radiation transfer models to retrieve vegetation canopy properties from remote sensing data, *J. Geophys. Res.*, *109*, D21205, doi:10.1029/2004JD005214.

Pinty, B., A. Lattanzio, J. V. Martonchik, M. M. Verstraete, N. Gobron, M. Taberner, J.-L. Widlowski, R. E. Dickinson, and Y. Goverts (2005), Coupling diffuse sky radiation and surface albedo, *J. Atmos. Sci.*, *62*(7), 2580–2591.

Rautiainen, M., P. Stenberg, T. Nilson, and A. Kuusk (2004), The effect of crown shape on the reflectance of coniferous stands, *Remote Sens. Environ.*, *89*, 41–52.

Ross, J. (1981), *The Radiation Regime and Architecture of Plant Stands*, 391 pp., Springer, New York.

Schaaf, C. B., et al. (2002), First operational BRDF, albedo and nadir reflectance products from MODIS, *Remote Sens. Environ.*, *83*, 135–148.

Sellers, P. J. (1985), Canopy reflectance, photosynthesis and transpiration, *Int. J. Remote Sens.*, *6*, 1335–1372.

Sellers, P. J., D. A. Randall, G. J. Collatz, J. A. Berry, C. B. Field, D. A. Dazlich, C. Zhang, G. D. Collelo, and L. Bounoua (1996), A revised land surface parameterization (SiB2) for atmospheric GCMs, Part I: Model formulation, *J. Clim.*, *9*, 676–705.

Sellers, P. J., et al. (1997), Modeling the exchanges of energy, water, and carbon between continents and the atmosphere, *Science*, *275*, 502–509.

Shaw, R. A., A. B. Kostinski, and D. D. Lanterman (2002), Super-exponential extinction of radiation on a negatively-correlated random medium, *J. Quant. Spectrosc. Radiat. Transfer*, *75*, 13–20.

Szczap, F., H. Isaka, M. Saute, B. Guillemet, and A. Ioltukhovski (2000), Effective radiative properties of bounded cascade absorbing clouds: Definition of an effective single-scattering albedo, *J. Geophys. Res.*, *105*, 20,635–20,648.

Verhoef, W. (1984), Light scattering by leaf layers with application to canopy reflectance modeling: The SAIL model, *Remote Sens. Environ.*, *16*, 125–141.

Vermote, E., D. Tanré, J. L. Deuzé, M. Herman, and J. J. Morcrette (1997), Second simulation of the satellite signal in the solar spectrum: An overview, *IEEE Trans. Geosci. Remote Sens.*, *35-3*, 675–686.

Verstraete, M. M. (1987), Radiation transfer in plant canopies: Transmission of direct solar radiation and the role of leaf orientation, *J. Geophys. Res.*, *92*, 10,985–10,995.

Verstraete, M. M., and R. E. Dickinson (1986), Modeling surface processes in atmospheric general circulation models, *Ann. Geophys.*, *4*, 357–364.

Verstraete, M. M., and B. Pinty (1997), Radiation transfer in SVAT models, in *Land-Surface Parameterization/Soil Vegetation-Atmosphere Transfer Schemes Workshop*, edited by H. Dolman and R. E. Dickinson, GEWEX technical report, pp. 31–39, *IGPO Publ. Ser.*, *31*.

Widlowski, J.-L., B. Pinty, N. Gobron, and M. M. Verstraete (2001a), Detection and characterization of boreal coniferous forests from remote sensing data, *J. Geophys. Res.*, *106*, 33,405–33,420.

Widlowski, J.-L., B. Pinty, N. Gobron, M. M. Verstraete, and A. B. Davies (2001b), Characterization of surface heterogeneity detected at the MISR/TERRA subpixel scale, *Geophys. Res. Lett.*, *28*, 4639–4642.

Widlowski, J.-L., M. M. Verstraete, B. Pinty, and N. Gobron (2003), Allometric relationships of selected European tree species, *Rep. EUR 20855 EN*, Joint Res. Cent., Ispra, Italy.

Widlowski, J.-L., B. Pinty, N. Gobron, M. M. Verstraete, D. J. Diner, and A. B. Davis (2004), Canopy structure parameters derived from multiangular remote sensing data for terrestrial carbon studies, *Clim. Change*, *67*, 403–415.

Yang, R., M. A. Friedl, and W. Ni (2001), Parameterization of shortwave radiation fluxes for nonuniform vegetation canopies in land surface models, *J. Geophys. Res.*, *106*(D13), 14,275–14,286.

Zeng, X., M. Shaikh, Y. Dai, R. E. Dickinson, and R. B. Myneni (2002), Coupling of the common land model to the NCAR community climate model, *J. Clim.*, *15*, 1832–1854.

Zhou, L., et al. (2003), Comparison of seasonal and spatial variations of albedos from Moderate Resolution Imaging Spectroradiometer (MODIS) and Common Land Model, *J. Geophys. Res.*, *108*(D15), 4488, doi:10.1029/2002JD003326.

———————————

R. E. Dickinson, School of Earth and Atmospheric Sciences, Georgia Institute of Technology, Atlanta, GA 30332, USA.

N. Gobron, T. Lavergne, B. Pinty, M. M. Verstraete, and J.-L. Widlowski, Global Vegetation Monitoring Unit, IES, EC Joint Research Centre, TP 440, via E. Fermi, I-21020 Ispra (VA), Italy. (bernard.pinty@jrc.it)